Excited State Processes in Solar Energy Materials

Österman, Tomas

2013

Excited State Processes in Solar Energy Materials

Tomas Österman

LUNDS
UNIVERSITET

DOCTORAL DISSERTATION
by due permission of the Faculty of Science, Lund University, Sweden.

To be defended at lecture hall G, Kemicentrum, Getingevägen 60, Lund,
Friday, June 14, 13.15.

Faculty opponent

Jouko Korppi-Tommola
Nanoscience Center of the University of Jyväskylä, Finland

Organization

Chemical Physics
Department of Chemistry
P.O. Box 124
SE-221 00 Lund
Sweden

Document name

DOCTORAL DISSERTATION

Date of issue

2013-05-21

Author(s)

Tomas Österman

Sponsoring organization

Title and subtitle

Excited State Processes in Solar Energy Materials

Abstract

This dissertation covers studies of excited state processes in two types of solar energy materials: alternating polyfluorene polymers and their blends with fullerenes in the active layer of plastic solar cells, and bis-tridentate Ru^{II}-polypyridyl complexes to be used as sensitizer in systems for artificial photosynthesis.

The polymer:fullerene blends were studied by transient absorption and time-resolved fluorescence measurements in order to investigate the role of the charge transfer (CT) state in charge formation. Previous studies have proposed that hot CT states is a necessary requirement for efficient charge formation in some active layer materials. However, in these studies relaxed CT states were shown to act as an intermediate state for at least ~20 % of the charges formed in the studied blends. This suggests that it is possible to achieve efficient charge formation without excess energy, which can lead to the development of solar cells with reduced energy losses.

Excited state properties of three bis-tridentate Ru^{II}-polypyridyl complexes with large variations in room-temperature lifetimes were studied by density functional theory (DFT) and time-dependent DFT calculations. Potential energy surfaces (PESs) calculated for the lowest triplet state were able to capture the decay channels responsible for the observed lifetime. The obtained activation energies for these decay processes were in reasonable agreement with experimental values. The PES calculations furthermore illustrated the importance of other features than the activation barriers in order to obtain a long room-temperature lifetime, in particular entropic factors seem to have significant contributions in some long-lived complexes. Improved understanding of the relation between chemical structure and room-temperature lifetime can lead to successful synthesis of long-lived complexes using other metals.

Keywords

Solar cells, Conjugated polymers, Charge transfer state, Time-resolved spectroscopy, Fluorescence, Artificial Photosynthesis, Bis-tridentate ruthenium(II)-complexes, Density functional theory, Quantum chemistry.

Classification system and/or index terms (if any)

Supplementary bibliographical information

Language

English

ISSN and key title

ISBN

978-91-7422-326-2

Recipient's notes

Number of pages

176

Price

Security classification

Signature _____ Date 14/5-13

Excited State Processes in Solar Energy Materials

Tomas Österman

Naturvetenskapliga fakulteten, Kemisk fysik
ISBN 978-91-7422-326-2

Tryckt i Sverige av Media-Tryck, Lunds universitet
Lund 2013

List of papers

This dissertation is based on the following papers, which will be referred to in the text by their Roman numerals. The papers are appended at the end of the dissertation.

I. **Geminate Charge Recombination in Polymer/Fullerene Bulk Heterojunction Films and Implications for Solar Cell Function**
S. K. Pal, T. Kesti, M. Maiti, F. Zhang, O. Inganäs, S. Hellström, M. R. Andersson, F. Oswald, F. Langa, T. Österman, T. Pascher, A. Yartsev and V. Sundström
Journal of American Chemical Society, **2010**, *132*, 12440-12451

II. **Ultrafast Spectroscopy Signature of Charge Transfer States in Polymer:fullerene Blends**
T. Österman, F. Zhang, O. Inganäs, V. Sundström and A. Yartsev
Submitted

III. **Time-resolved Fluorescence Reveals Dissociation of Relaxed Charge Transfer States in Polymer:fullerene Blends**
T. Österman, K. Tvingstedt, Z. Tang, K. Vandewal, O. Inganäs, T. Pascher, V. Sundström and A. Yartsev
Manuscript

IV. **Bistridentate Ruthenium(II)polypyridyl-Type Complexes with Microsecond ^{3}MLCT State Lifetimes: Sensitizers for Rod-Like Molecular Arrays**
M. Abrahamsson, M. Jäger, R. J. Kumar, T. Österman, P. Persson, H.-C. Becker, O. Johansson and L. Hammarström
Journal of American Chemical Society, **2008**, *130*, 15533-15542

V. **Influence of Triplet State Multidimensionality on Excited State Lifetimes of Bis-tridentate Ru^{II} Complexes: A Computational Study**
T. Österman, M. Abrahamsson, H.-C. Becker, L. Hammarström and P. Persson
Journal of Physical Chemistry A, **2012**, *116*, 1041-1050

VI. **Excited State Potential Energy Surfaces of Bistridentate Ru^{II} Complexes – A TD-DFT Study**
T. Österman and P. Persson
Chemical Physics, **2012**, *407*, 76-82

Papers related to but not included in this dissertation.

VII. **A 3.0 µs Room Temperature Excited State Lifetime of a Bistridentate Ru[II]-polypyridine Complex for Rod-like Molecular Arrays**
M. Abrahamsson, M. Jäger, T. Österman, L. Eriksson, P. Persson, H.-C. Becker, O. Johansson and L. Hammarström
Journal of American Chemical Society, **2006**, *128*, 12616-12617

List of contribution

I. I was responsible for the TCSPC measurements and contributed largely to that part of the paper. I had only very minor contributions to the other parts of the paper.

II. I planned and carried out all the experiments, did all analysis and was the main author of the paper.

III. I planned and carried out all streak camera experiments and a major part of the steady-state experiments. I did all analysis and was the main author of the paper.

IV. I carried out all the calculations, did all analysis of the calculations and had minor contributions to the text.

V. I shared responsibility for the planning, carried out some of the calculations, participated in the analysis and was one of the main contributors to the paper.

VI. I participated in the analysis and shared responsibility for writing the paper.

Abbreviations

[70]BTPF	3′-(3,5-bis-trifluoromethylphenyl)-1′-(4-nitrophenyl)pyrazolino [70]fullerene
[70]PCBM	[6,6]-phenyl-C71-butyric acid methyl ester
APFO	alternating polyfluorene
B3LYP	three-parameter hybrid functional
bmp	6-(2-picolyl)-2,2′-bipyridine
CT	charge transfer
DFT	density functional theory
DPA	donor-photosensitizer-acceptor
dqp	2,6-di(quinolin-8-yl)pyridine
DSSC	dye-sensitized solar cell
HOMO	highest occupied molecular orbital
IC	internal conversion
ISC	intersystem crossing
LBO	lithium triborate
LUMO	lowest unoccupied molecular orbital
MC	metal-centered
MLCT	metal-to-ligand charge transfer
MO	molecular orbital
NOPA	noncollinear optical parametric amplifier
OD	optical denisty
PCBM	[6,6]phenyl-C61-butyric acid methyl ester
PES	potential energy surface
SPAD	single photon avalanche diode
TCSPC	time-correlated single photon counting
TDDFT	time-dependent DFT
tpy	2,2′:6′,2″-terpyridine
VR	vibrational relaxation

Contents

1. Introduction

There is a historical coupling between economic development and increasing energy usage. This has eventually resulted in a substantial rise in the emission of greenhouse gases, which is believed to be the major factor behind today's alarming rate of global warming and climate change. As the economic development is expected to continue, and in fact even accelerate in many parts of the world, there is an urgent need to break the correlation between economic development and emission of greenhouse gases. Renewable energy provides one of the means to achieve this decoupling, particularly energy sources relying on direct solar energy as the solar irradiance at the surface of the Earth corresponds to an energy supply almost 8,000 times the world's primary energy consumption in 2008. If practical limitations of solar energy technology are taken into account, the potential energy supply is still estimated to be 3 to 100 times the world's primary energy consumption.[1]

This doctoral dissertation will focus on two different types of direct solar energy: electricity generation through conversion of sunlight by solar cells, and solar fuel generation through conversion of sunlight to hydrogen gas by photochemical reactions mimicking natural photosynthesis. During operation of both these types of systems, similar photoinduced processes occur in their respective active materials. First, an excited state is formed by the absorption of a photon by the light-harvesting component. If the photon is not directly absorbed at an electron transfer site, the excited state undergoes energy transfer to such a site. At the site, an electron and a corresponding hole are formed via electron transfer to an electron accepting species. The electron and hole then separate into free charges, which can be extracted in an external circuit or participate in the reduction of protons to hydrogen.

A new generation of solar cells, offering high flexibility and low cost production, is emerging.[2,3] One of the promising alternatives in this new generation are plastic solar cells[4], i.e. cells whose active material consists of a blend of a conjugated polymer (electron donor) and an electron accepting molecule, typically a fullerene derivate.[5,6] The absorption of light primarily occurs in the polymer, thus acting as the light harvester, and charge formation occurs through electron transfer at the polymer-fullerene interface. Depending on the character of the blend and the intermixing of the polymer and the fullerene, extensive phases of neat polymer can

be present in the blend. In such cases, energy transfer within the polymer phase to a fullerene interface is required before charges can be formed.[7] After charge formation, the electron and hole are transported in the fullerene and polymer phases, respectively, to the electrodes of the cell.

Another type of solar cell belonging to the new generation are dye-sensitized solar cells (DSSCs). These consist of a porous semiconductor, typically TiO_2, sensitized by dyes covalently bound to the TiO_2 surface. The sensitization is needed in order to increase the otherwise poor light harvesting of TiO_2, which has a very blue absorption onset at about 400 nm[8], and can be achieved by using transition metal complexes, typically Ru^{II}-polypyridyl complexes. This design ensures close proximity between the electron donor and acceptor and therefore usually results in efficient and ultrafast electron transfer from the dye to the TiO_2, from where the electron is easily transported to the electrode.[8-12] In contrast to the polymer solar cells, an electrolyte is needed to regenerate the oxidized dye and to transport the hole to the anode of the cell. The electrolyte brings problems related to a relatively high potential drop in the regeneration process, recombination with electrons in the TiO_2, temperature stability, and hazardous solvents, and can therefore currently be considered as a limiting factor for the introduction of DSSCs in commercial applications.[8] Transition metal complexes can also be applied as photosensitizers in the field of solar fuel.[13] In particular, complexes with bis-tridentate ligands are of interest as these, through substitutions along the pseudo-C_2 axis, offer synthetic strategies to achieve covalently bound DPA-type (Donor-Photosensitizer-Acceptor) molecular arrays for vectorial electron transfer (Figure 1.1).[14] After excitation of the photosensitizer, electron transfer to the acceptor leads to the intermediate charge separated state DP^+A^-. A subsequent hole transfer to the photosensitizer from the donor results in the fully charge separated state D^+PA^-, which then can participate in the production of hydrogen. Electron transfer in DPA triads is usually considerably slower than in the DSSCs[15], making a long excited state lifetime of the photosensitizer a necessary requirement to reach high energy conversion efficiencies.

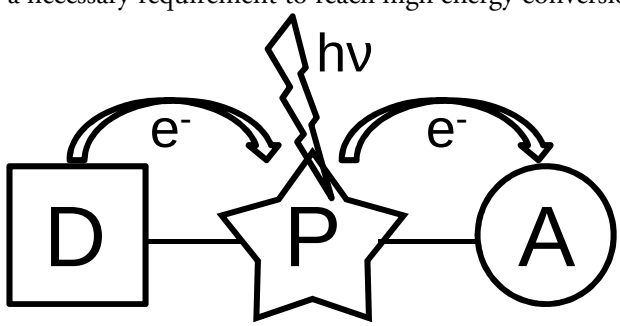

Figure 1.1. Schematic picture of a covalently bound DPA molecular array. Light absorption in the photosensitizer, P, is followed by two subsequent electron transfer processes to give the fully separated state where the donor, D, has oxidizing capacity and the acceptor, A, has reducing capacity.

In order to improve the performance of the systems described above, knowledge about the excited state dynamics is essential. Models of many key processes already exist, but there are still fundamental questions left to be answered. The studies presented in this doctoral dissertation aim to address some of these questions, and to develop the understanding of the mechanisms governing the performance of plastic solar cells and the excited state lifetime of bis-tridentate Ru^{II}-polypyridyl complexes. This will hopefully lead to the development of new materials with improved properties for solar energy conversion.

Charge generation in polymer:fullerene blends involves a charge transfer (CT) state, which furthermore is directly related to the solar cell performance via a strong coupling to the open circuit voltage.[16,17] The role of the CT state in the conversion of polymer excitons to extractable charges is investigated by employing ultrafast time-resolved transient absorption and fluorescence techniques. The primary systems of study in this part are films and solar cells based on blends of alternating polyfluorene polymers and PCBM ([6,6]phenyl-C61-butyric acid methyl ester).

Whereas the size and heterogeneity of the polymer:fullerene system makes it rather challenging to investigate by means of quantum chemical calculations[18], many metal-polypyridyl complexes allow for such studies. Therefore, density functional theory calculations on bis-tridentate Ru^{II}-polypyridyl complexes that can be used in molecular DPA arrays are employed to characterize the properties of the triplet metal-to-ligand charge transfer (^{3}MLCT) and metal centered (^{3}MC) states. The experimentally well-studied ^{3}MLCT state possesses electronic properties that are favorable for energy or electron transfer.[19] In particular the lifetime is crucial, and this study has thus focused on the deactivation dynamics of the ^{3}MLCT state via the experimentally elusive ^{3}MC state.

1.1 Outline of the doctoral dissertation

This doctoral dissertation consists of five parts (corresponding to chapters 2-6). The first part provides a background to the properties and dynamics of excited states used in the following parts. Part two briefly describes and discusses the experimental techniques and theoretical methodologies used in the studies. Part three and four cover the studies on polymer-based films and Ru^{II}-based sensitizers, respectively, with a summary and evaluation of the obtained results. The last part includes final considerations spanning both of the studied systems.

2. Properties and dynamics of excited states

The excited state properties of the studied systems are, as mentioned in the introduction, of principal importance for the final target of solar energy conversion; they govern which processes occur and their dynamics (i.e. how they occur). This chapter first provides a general overview on the nature of electronic states in molecules and on light-induced processes within and between these states. It is then further described how these processes couple to the excited state properties and the experimentally observed kinetics.

2.1 Electronic states of molecules

An electron configuration of a molecule describes how its electrons are distributed in the molecular orbitals (MOs), and each configuration corresponds to a specific electronic state. The properties of a state, for example the energy and the multiplicity, are thus governed by the character and population of the MOs. The multiplicity is given by the total angular spin momentum, S, according to $2 \cdot S + 1$. All unpaired electrons contribute with ½ to S, usually resulting in singlet multiplicity of the ground state as all occupied MOs of the ground state in most cases are doubly populated by two electrons with opposing spin. The most well-known exception is the ground state of molecular oxygen, O_2, where the HOMO consists of two degenerate MOs with one electron in each, giving a triplet multiplicity. This is in accordance with Hund's first rule, which states that the state with highest multiplicity also corresponds to the state with lowest energy.

When the interaction of a molecule with its surroundings is of interest, particular importance is put on the properties of the frontier orbitals: the highest occupied molecular orbital (HOMO) and the lowest unoccupied molecular orbital (LUMO). That is also the case for absorption of light in the visible wavelength region, which is the region of largest interest for solar energy applications, where transitions typically involve the valence electrons of the molecules, including the frontier orbitals and energetically close-lying MOs. Absorption corresponds to a transition

from the ground state to another electronic quantum state, an excited state, and the energy of the absorbed photon has to match the energy difference between the ground state and the excited state (including excited vibrational levels). The lowest transition in a molecule can, in the simplest cases, be described as moving one electron from HOMO to LUMO.

2.2 Light-induced processes

The processes occurring in molecules after light absorption[20] are usually illustrated by a Jablonski diagram[21], see Figure 2.1. Absorption of a photon brings, as described above, the ground state to a singlet state that is both electronically and vibrationally excited. Vibrational relaxation (VR) leads to rapid (hundreds of fs) dissipation of energy and results in the population of the lowest vibrational level of the excited state. If any lower excited states are present, internal conversion (IC; in the case of conversion to a state of the same multiplicity) and intersystem crossing (ISC; in the case of conversion to a state of a different multiplicity) leads to population of these. Both IC and ISC are vibrationally mediated, but their respective characteristic timescales are usually distinctly different. IC is normally very fast (hundreds of fs), and most subsequent excited state processes, such as radiative processes, will thus occur from the lowest vibrational level of the lowest singlet excited state. ISC involves spin flipping (requiring magnetic interactions provided by spin-orbit coupling) and is therefore associated with longer timescales. However, strong spin-orbit coupling can result in high enough ISC rates to compete with VR and IC. IC and ISC are also viable non-radiative routes for repopulation of the ground state, even if transitions to the ground state generally are much slower than transitions to other excited states as the amount of energy

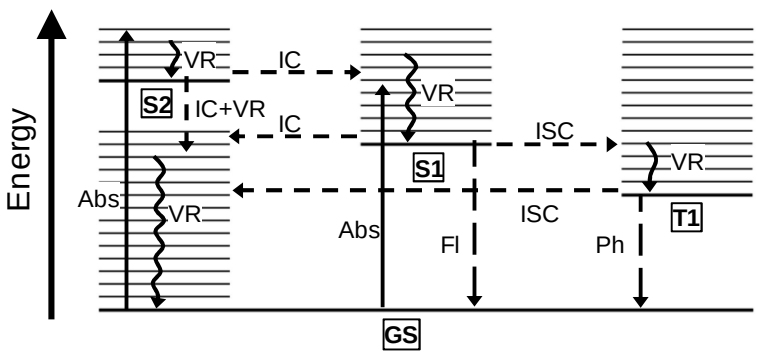

Figure 2.1. Jablonski diagram illustrating the most common photoinduced processes in molecules: absorption (Abs), vibrational relaxation (VR), internal conversion (IC), intersystem crossing (ISC), fluorescence (Fl) and phosphorescence (Ph). Note that the shift of S1 and T1 only is for clarity.

that needs to be dissipated is considerably higher. Radiative repopulation of the ground state occurs through fluorescence (Fl) from singlet states and through phosphorescence (Ph) from triplet states. Typical fluorescence lifetimes are on the order of ns whereas phosphorescence, which requires spin flipping, typically occurs on the μs – ms timescale.

It is obviously desirable to maximize the sunlight harvesting for solar energy purposes. However, the absorption onset must match the energy needed to achieve optimum performance of the system, which inevitably results in transmission of the photons of lower energy. Furthermore, the excess energy of photons of higher energy is also lost as a result of fast internal relaxation (VR and IC). For example, the detailed balance limit developed for an ideal single-junction cell at 300 K by Shockley and Queisser[22] allows for the estimation of the optimum absorption onset for solar cells to just above 900 nm, leading to a ~55 % loss of the total AM 1.5 solar energy solely by transmission and relaxation processes[23,24], see Figure 2.2. AM 1.5 is the standard solar spectrum used for efficiency measurements of solar cells, and the theoretical maximum efficiency with an absorption onset at 1100 nm when also taking recombination into account is ~31 %.[22] Efforts along various pathways to overcome this limitation are pursued.[25]

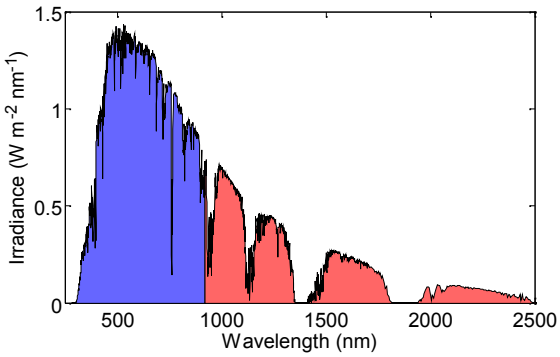

Figure 2.2. AM 1.5 spectrum obtained from http://rredc.nrel.gov/solar/spectra/am1.5/. The purple and red parts of the spectrum correspond to the wavelengths above and below the optimum single-junction absorption onset, respectively.

2.3 Excited state reaction rates and dynamics

The light-induced processes described above are first-order reactions, and the population, P_t, of the involved states at time t thus evolves with the first-order reaction rate, k, according to the integrated first-order rate law:

$$P_t = P_0 \cdot \exp(-kt) \qquad (2.1)$$

where P_0 is the initial population.

Information about the dynamics can be extracted by studying the temperature-dependence of the reaction rate. The obtained data can then be analyzed using Arrhenius' equation:

$$k = A \cdot \exp(-E_a/(RT)) \qquad (2.2)$$

where R and T are the ideal gas constant and the temperature, respectively. E_a is the activation energy for the reaction and the pre-exponential factor A is the frequency factor, which contains information about the number of favorable geometrical arrangements of the nuclei per unit time. The value of A for excited-state processes is thus strongly connected to the vibrations and the entropy of the system. Both E_a and A provide information about the dynamics of the process and can be represented in a reaction coordinate diagram where one, or several, coordinates of the nuclei describe the reaction pathway for the studied process. The coordinates should be chosen to capture the reaction pathway of study. A reaction coordinate diagram consisting of more than one coordinate will result in a potential energy surface (PES) of the same dimension as the number of coordinates. A schematic example of a one-dimensional reaction coordinate diagram between two states described by harmonic oscillators is shown in Figure 2.3.

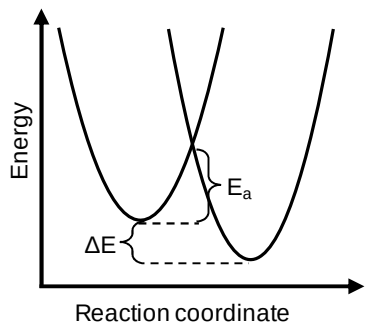

Figure 2.3. Schematic illustration of a one-dimensional reaction coordinate diagram between two crossing states. The forward crossing process has an activation energy E_a and a driving force ΔE (neglecting entropic effects).

The lifetime, τ, of a reaction is defined as the time it takes for the population to fall to 1/e of its initial value. The lifetime of first-order processes is connected to the reaction rate via $\tau = 1/k$. However, it is often more interesting to consider the experimentally observed lifetime, τ_{obs} (equation 2.3), which depends on the sum of the reaction rates coupled to all the processes, i, that deplete the studied population. Such processes will always lead to a decrease of the lifetime and they are therefore referred to as quenching processes. The amount of the total population that goes via the studied route, n, is given by the quantum yield, Φ_n (equation 2.4). The

expressions for the observed lifetime and the quantum yield will be further complicated if also the processes leading to an increase of the studied population, such as equilibria or consecutive reactions, have to be taken into account.

$$\tau_{obs} = 1/k_{obs} = 1/\Sigma k_i \quad (2.3)$$

$$\Phi_n = k_{i=n}/\Sigma k_i \quad (k_{i=n} = k_{obs}) \quad (2.4)$$

2.4 Absorption and emission

Absorption is the result of the interaction between matter and the electric field component of an electromagnetic field, i.e. light. This dissertation will, as explained in chapter 1, consider excited state processes induced by absorption in the 300-1000 nm wavelength range, which corresponds to the visible (and some UV and near-IR) light. Absorption of such photons promotes one electron from an occupied electronic state of a molecule to an unoccupied electronic state of higher energy. The energy difference between the initial and the final state must, because of energy conversion, match the energy of the absorbed photon.

Different excited states will, depending on their coupling to the initial state, interact more or less with the electromagnetic field, giving rise to an absorption spectrum consisting of wavelength-dependent peaks of different intensities corresponding to each transition. The intensity of the absorption at a specific wavelength, λ, is usually measured in terms of the absorbance, A_λ, given by the Beer–Lambert law:

$$A_\lambda = \log(I_{0,\lambda}/I_\lambda) = \varepsilon_\lambda \cdot c \cdot l \quad (2.5)$$

where $I_{0,\lambda}$ is the incident intensity, I_λ the transmitted intensity, ε_λ the extinction coefficient, c the concentration of the sample, and l the path length of the light through the sample. It follows from equation 2.5 that in order for the absorbance to be excitation intensity independent, the absorption has to scale linearly with intensity. This is the case for most materials under non-extreme excitation conditions, and absorption is therefore sometimes referred to as linear absorption.

Emission corresponds to the reverse phenomenon of absorption; a radiative transition from a higher-lying state to a lower. Fluorescence corresponds to the case when the transition occurs between states of the same multiplicity whereas phosphorescence corresponds to transitions between states of different multiplicity (see Figure 2.1). As both fluorescence and phosphorescence normally are much slower processes than VR and IC, the emission typically occurs from the lowest excited state of a given multiplicity. This is known as Kasha's rule.[26]

2.4.1 Stokes shift

Kasha's rule together with the Franck-Condon principle, which states that an electronic transition occurs much faster than the motion of the nuclei and thus can be considered as a vertical transition, leads to a peak shift between absorption and emission. This can be illustrated in a coordinate diagram for two states described by Morse potentials (which, in contrast to the harmonic potentials in Figure 2.3 account for bond breaking and some anharmonicity), see Figure 2.4. First, ground state absorption at the relaxed ground state geometry, corresponding to the coordinate Q_{GS}, leads to the population of a vibrationally hot level of the excited state. The excited state then undergoes VR to its relaxed geometry, corresponding to Q_{ES}, before it decays through fluorescence to a vibrationally hot level of the ground state. Finally, the ground state returns to its relaxed geometry through VR. The VR processes, which partly depend on the shift between Q_{GS}, and Q_{ES}, give a red-shift of the fluorescence compared to the absorption. This is referred to as a Stokes shift.

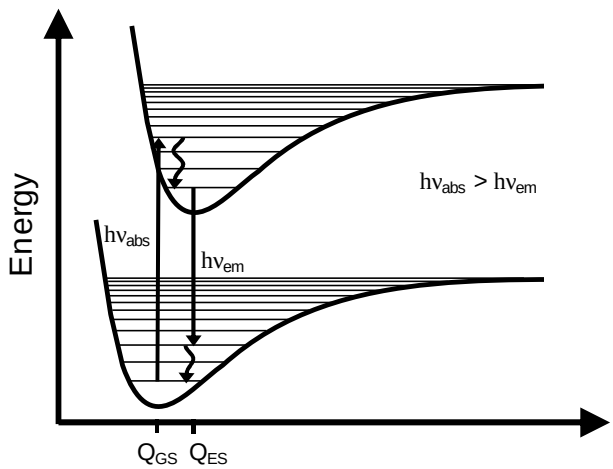

Figure 2.4. A Morse potential energy diagram illustrating the origin of the Stokes shift in terms of energy loss by VR and geometrical rearrangement.

2.5 Energy and electron transfer

Both energy transfer and electron transfer correspond to the migration of energy from a donor site to an acceptor site (Figure 2.5). Electron transfer occurs through the actual movement of an electron from its corresponding hole, and results in a reduced donor and an oxidized acceptor. As such, it is crucial for the charge formation and separation in artificial photosynthesis and plastic solar cells. Electron

transfer is usually described using Marcus theory, but it will not be given any further treatment here as it is not explicitly dealt with in this dissertation. Energy transfer can be relevant in artificial photosynthesis[27] and is definitely one of the most prominent features of conjugated polymers.[28] It results in the de-excitation of the donor and excitation of the acceptor, i.e. migration of the excited state from one chromophore to another. The type of energy transfer relevant for these systems is usually Förster energy transfer, which occurs through non-radiative dipole-dipole coupling at a rate given by:

$$k_{EnT} = k_D \cdot \Phi_D \cdot \kappa^2 / r^6 \cdot (9000 \cdot \ln(10) / (128 \cdot \pi^5 \cdot N_A \cdot n^4)) \cdot J \qquad (2.6)$$

where k_D is the decay rate of the donor in the absence of the acceptor, Φ_D the quantum yield of the donor in the absence of the acceptor, κ^2 a factor describing the relative orientation of the transition dipoles of the donor and acceptor (ranges between 0 and 4, and is equal to 2/3 for random orientations), r the distance between donor and acceptor, N_A Avogadro's number, n the refractive index of the medium, and J the overlap integral over all wavelengths given by:

$$J = \int F_D(\lambda) \cdot \varepsilon_A(\lambda) \cdot \lambda^4 d\lambda \qquad (2.7)$$

where F_D is the fluorescence spectrum of the donor with the total intensity (area under curve) normalized to unity, and ε_A the extinction coefficient of the acceptor given in $M^{-1} \cdot cm^{-1}$.[29] Energy transfer will, as a result of the Stokes shift, in most cases lead to downhill energy migration.

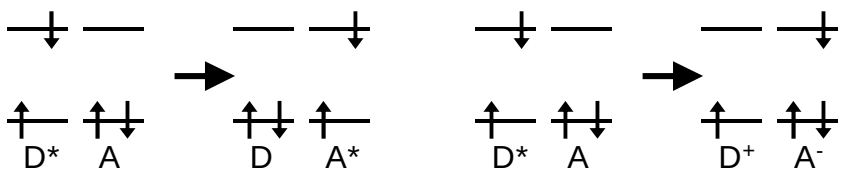

Figure 2.5. Illustration of energy transfer (left) and electron transfer (right) from a donor, D, to an acceptor, A.

3. Techniques and methodology

In this chapter the time-resolved spectroscopic techniques used to investigate the polymer-based blends and the theoretical methodology employed to characterize the Ru^{II}-based sensitizers are briefly described and discussed. Ultrafast transient absorption measurements have been used to study processes on sub-100 fs timescales and longer. These have been complemented by time-resolved fluorescence experiments that give worse time resolution but instead provide the opportunity to only study the fluorescent states: streak camera measurements (~2 ps time resolution) and time-correlated single-photon counting measurements (~50 ps time resolution). The time-resolved measurements have in turn been complemented by steady-state absorption and fluorescence measurements using standard commercial spectrometers (Agilent UV-visible spectrometer and Spex Fluorolog spectrometer), not described in further detail. All quantum chemical calculations have been based on density functional theory, which is the most commonly employed quantum chemical method for accurate calculations of large molecules, and were performed with the Gaussian program package.[30]

3.1 Transient absorption

Ultrafast transient absorption is a pump-probe technique that utilizes short laser pulses (< 100 fs) to monitor excited-state processes of molecules and materials. Linear steady-state absorption (equation 2.5) is measured by relating the transmitted intensity of the probe through the sample, I, to the transmitted intensity of a reference, I_r (equation 3.1). In pump-probe measurements, every second probe pulse is spatially and temporally overlapping with a pump pulse that excites the sample, giving rise to transmitted intensity, I^*, and absorbance, A^*, related to the photoinduced species. The differential absorption, ΔA, can then be calculated using equation 3.2. The pump-induced transients are finally measured by introducing and changing a controllable temporal delay between the pump and the probe pulses. Probing at times and wavelengths where the excited state absorption is dominating will thus result in $I^* < I$ and a positive ΔA signal. For cases where ground state bleach or stimulated emission is dominating, consequently a negative ΔA signal will be obtained.

$$A = A - A_r = \log(I_0/I) - \log(I_0/I_r) = \log(I_r/I) \quad (3.1)$$

$$\Delta A = A^* - A = \log(I_r/I^*) - \log(I_r/I) = \log(I/I^*) \quad (3.2)$$

A schematic drawing of the transient absorption set-up is shown in Figure 3.1. A laser system (Clark) consisting of a Ti:Sapphire regenerative amplifier, pulse compressor, and an Nd:YAG pump laser head provided pulses with a repetition rate of 1 kHz at a wavelength of 775 nm. The output was split into two fractions, one that was taken into a noncollinear optical parametric amplifier (NOPA) to generate the pump pulses and one of which was sent into another NOPA to generate the probe pulses. Both pulses were compressed in order to obtain a time resolution of ~30 fs. The repetition rate of the pump was reduced to 500 Hz using a chopper, and it was then passed through a Berek compensator and a polarizer before exciting the sample. The probe was split into two parts: one reference directed straight to the detector (giving I_r), and one probe taken through the sample and then to the detector. Transient spectra were measured with ~200 nm broad probe pulses and diode array detectors, whereas transient kinetics was measured using close to transform-limited probe pulses and photodiode detectors. Two variational delay stages were used to vary the time delay between pump and probe: one 20 ns delay stage (~1 ps time resolution) and one 500 ps delay stage (~0.3 ps time resolution).

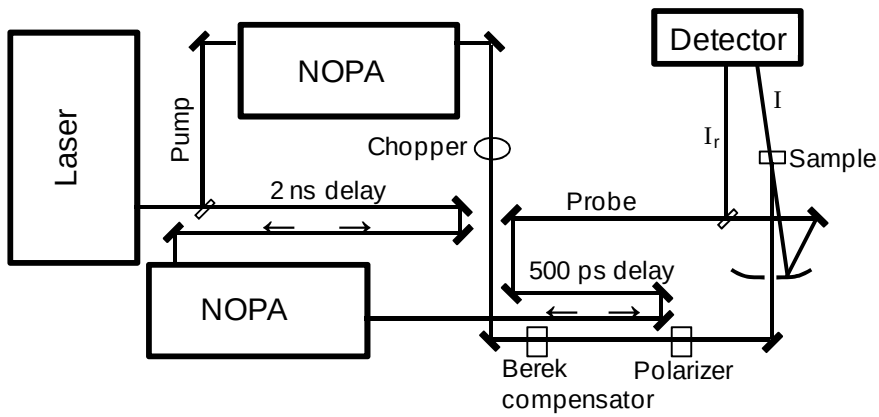

Figure 3.1. Schematic illustration of the transient absorption set-up.

3.2 Streak camera

A streak camera set-up is used to measure time-resolved photoluminescence on timescales down to a few ps. It consists of a spectrograph for spectral resolution and the streak camera itself for temporal resolution. The emission is focused onto a vertical slit (variable in the horizontal plane) before entering the spectrograph where the gratings provide spectral separation in the horizontal plane. The focusing plane of the spectrograph output is set at the input horizontal slit (variable in the vertical plane) of the streak camera. A second set of collimating and focusing optics is then used to image the photons from the second slit on a photocathode. When photons hit the photocathode, photoelectrons are created nearly instantaneously with a spatial distribution in the horizontal plane according to the incoming photon density. These are then accelerated into the streak tube, where a very fast sinusoidally time-dependent streak voltage is locally applied in the vertical direction leading to a deviation along in the vertical plane. As the applied voltage is changed very quickly, the extent of the electron deviation is determined by the timing of the photoelectrons arriving in the region of applied field. The time-dependent photoelectron deviation is then converted in a vertical position at the plane of a microchannel plate electron detector. The microchannel plate is used to resolve the position of the photoelectrons and to amplify the electrons before they hit the phosphor screen, which converts them back to photons that can be detected by a CCD camera. As a result, a two-dimensional image with spectral resolution on the horizontal axis and temporal resolution on the vertical axis is obtained. The temporal resolution can be varied by changing the horizontal slit and the amplitude of the streak voltage. The sine function of the voltage is synchronized with the repetition rate of the laser, which is fed in through a fast photodiode.

A schematic drawing of the streak camera set-up is shown in Figure 3.2. The laser system consisted of a 532 nm laser (Millennia Pro) pumping a passively mode-locked Ti:Sapphire oscillator (Tsunami), typically providing ~100 fs pulses at 80 MHz repetition rate with a wavelength of 800 nm. A small portion of the output was redirected to the trigger photodiode while the rest was frequency doubled using a lithium triborate (LBO) crystal. The resulting blue (400 nm) beam was taken through a shortpass filter, a variable neutral density filter and an elevating periscope before it was used for unfocused excitation of the sample in a front-face geometry. The fluorescence was collimated, passed through a polarizer set a magic angle and focused onto the entrance slit of the spectrograph (Chromex). Both the streak camera and the CCD are Hamamatsu products.

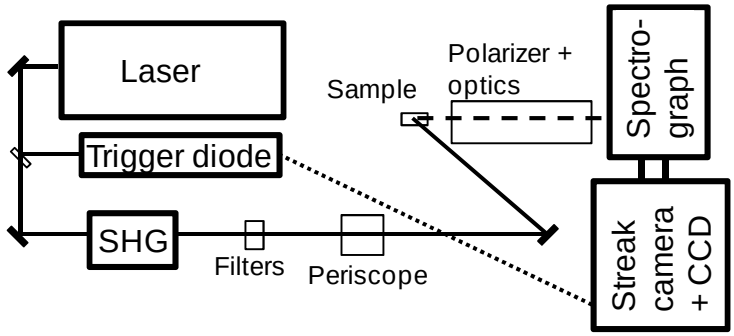

Figure 3.2. Schematic illustration of the streak camera set-up.

3.3 Time-correlated single-photon counting

Time-correlated single-photon counting (TCSPC) is based on binning of the time arrival of the detected fluorescence photon compared to the start signal into a histogram. The start signal is provided by a laser-triggered photodiode and the resulting histogram should thus report on the fluorescence lifetime. The signal processing is carried out in a Time to Digital Converter, which can provide a time resolution of a few tens of ps. It is important to keep the detected counting rate much lower than the repetition rate of the laser in order to avoid pile up of the signal.

A schematic drawing of the TCSPC set-up is shown in Figure 3.3. A diode laser head connected to a laser driver (PicoQuant) provided ~200 ps laser pulses at 405 nm. A rather unconventional direct excitation scheme, where the sample is located as close to the detector as possible, was used to allow for non-focused excitation light. Three filters (two longpass and one bandpass filters) were placed in between of the sample and the detector in order to block out residual (excitation) light and to select the wavelength region of interest. The detector was a single photon avalanche diode (SPAD, Micro Photon Devices) and the start signal was directly supplied by the laser driver. Both start and stop signals were connected to a PicoQuant PicoHarp 300, which implemented the time binning and the calculation of the histogram.

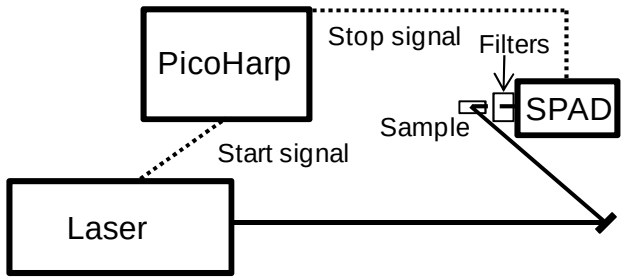

Figure 3.3. Schematic illustration of the TCSPC set-up.

3.4 Quantum chemical calculations

Quantum chemical calculations provide a tool for fundamental understanding of the properties of molecules and matter, and can hence be used to, for example, describe intra- and intermolecular interactions and interactions with electromagnetic waves such as light. Depending on the approach, different levels of theory and accuracy can be reached. A general rule is that increasingly accurate methods scale increasingly with the size of the system. It is therefore important to find a level of theory that describes the system well enough in respect to the properties of interest, and that still is computationally manageable. Density functional theory (DFT) has in many cases been shown to describe the properties of the ground state and the lowest excited states of transition metal complexes to a satisfactory level[31-33], and has thus been our choice of method for the studies of bis-tridentate Ru^{II}-polypyridyl complexes. Before describing DFT, a short background on quantum chemical calculations in general will be presented. It will be based on the books of Szabo and Ostlund[34], and Jensen.[35]

Quantum chemical calculations aim to solve the time-independent non-relativistic Schrödinger equation of the total wave function, $\Psi_{tot}(R,r)$. The calculations are usually performed within the adiabatic Born-Oppenheimer approximation, which decouples the electrons from the nuclei based on the nuclei being much heavier than the electrons. This means that $\Psi_{tot}(R,r)$ can be written as a product of the nuclear wave function, $\Psi_n(R)$, and the electronic wave function, $\Psi_e(R,r)$, as:

$$\Psi_{tot}(R,r) = \Psi_n(R)\cdot\Psi_e(R,r) \qquad (3.3)$$

where R are the nuclear coordinates and r the electronic coordinates. The electrons can thus be considered as moving in a fixed field stemming from the nuclei, and it is possible to calculate the energy, $E_e(R)$, of the electronic wave function using a specific set of the nuclear coordinates R. If also the nuclear repulsion is included in

$E_e(R)$, one can address the motion of the nuclei within the average electronic potential according to the nuclear Schrödinger equation:

$$(\mathbf{T}_n + E_e(R))\cdot\Psi_n(R) = E_{tot}\cdot\Psi_n(R) \quad (3.4)$$

where $\mathbf{T}_n$ is the nuclear kinetic energy operator and E_{tot} the total energy of the system. The electronic energy thus works as a potential that depends on the nuclear coordinates, leading to the view of the nuclei as moving on a PES given by $E_e(R)$. This means that the electronic Schrödinger equation has to be solved for a specific set of nuclear configurations in order to obtain the nuclear dynamic properties and structures as well as the electronic properties.

The electronic wavefunctions are normally described by MOs, which are constructed by a linear combination of atomic orbitals provided from a chosen basis set of one-electron spinorbitals in terms of a single Slater determinant.[36] They are then optimized in an iterative way until the total energy has converged below a certain threshold. This is justified by the variational principle: an approximate wave function can never have lower energy than the exact one. As a result, the electrons are treated independently of each other, moving in an average field of all other electrons and nuclei. However, the electron-electron repulsion is thus only accounted for in an average way, giving rise to a neglect of electron correlation. As will be explained below, DFT aims to recover the resulting energy difference (the correlation energy) by the means of exchange-correlation functionals.

3.4.1 Density functional theory

This part will briefly describe and discuss DFT and is mostly based on the descriptions provided by Baerends and Gritsenko[37] and Piela.[38] The fundamental concept of DFT is to consider the electron density, $\rho(r)$, of all N electrons moving in the potential field of fixed nuclei, $v(r)$, rather than considering individual electrons and their respective MOs. The density determines the probability of finding any electron within a certain volume. Hohenberg-Kohn formulated two theorems which made calculations using ρ possible.[39] The first theorem states that the ground state electronic wave function, Ψ_0, corresponds to one unique ρ (ρ_0), and vice versa. It furthermore states that Ψ_0 and ρ_0 also correspond to one unique v, and vice versa. Consequently, all properties, including the energy, of the system are functionals of ρ. The second theorem states that the variational principle is valid for the ground state energy expressed as a functional of ρ_0 as well. These two theorems hence allows for calculations of the ground-state wave function using ρ_0 and the iterative procedure following from the variational principle by minimizing the energy in the external potential v, $E_v[\rho_0(r)]$. However, difficulties to find an explicit expression for ρ_0 lead to the implementation of the Kohn–Sham formulation of DFT.[40]

The Kohn-Sham formulation introduces wave functions by assuming that all the N electrons in the system do not interact but are instead influenced by an external local potential, $v_s(r)$. The external potential is constructed such that its wave function will consist of a Slater determinant with the dimension N, and that it still results in the same electron density as would be the case if v was used, i.e. the obtained ρ equals ρ_0. One then only has to solve the one-electron equation:

$$(-\Delta/2 + v_s)\cdot\varphi_i = \varepsilon_i\cdot\varphi_i \qquad (3.5)$$

where Δ is the del squared operator and φ_i are the so-called Kohn-Sham spin orbitals. The first term in the parenthesis in equation 3.5 corresponds to the kinetic energy of the electrons. So far no further approximations have been introduced and the resulting ρ, which equals the sum of the orbital densities, is the exact one. Equation 3.5 is solved by the means of the variational principle where its total energy is minimized. The energy is in turn given by:

$$E[\rho] = E_{Ne}[\rho] + T[\rho] + J[\rho] + E_{XC}[\rho] \qquad (3.6)$$

where $E_{Ne}[\rho]$ is the Coulombic electron-nuclei interaction, $T[\rho]$ the electronic kinetic energy of the non-interacting electrons, $J[\rho]$ the electrostatic repulsion energy from interaction of the electron cloud with itself, and $E_{XC}[\rho]$ the exchange–correlation energy. The E_{XC} term includes the energy related to the exchange interaction and correlation of the electrons as well as the part of the kinetic energy not included in $T[\rho]$, and is thus the only unknown of this equation. As a consequence it has to be guessed or estimated. There are numerous functionals available; for investigations of the excited states of transition metal complexes so-called hybrid functionals have shown to be successful.[31]A major part of the calculations on Ru^{II}-polypyridyl complexes presented in this dissertation are based on the B3LYP functional.[41]

Only the ground state has been dealt with so far, and DFT is in fact primarily optimized for ground state calculations. However, it has been shown that DFT also can be used to investigate the lowest lying state, i.e. the corresponding ground state, of each spatial or spin irreducible representation of the system.[31,42] The adiabatic approximation introduced above does, on the other hand, introduce problems when considering states that are close in energy. In those cases the Born-Oppenheimer approximation is no longer valid, and non-adiabatic processes leading to avoided crossings (or conical intersections), instead of the adiabatic crossings suggested by the DFT calculations, are more appropriate descriptions of the dynamics in such regions. DFT calculations can nonetheless provide important information about the approximate energies and coordinates in this region, even if the actual crossing is poorly described. If higher excited states than the lowest state of the spatial or spin irreducible representation are to be explored, time-dependent DFT (TDDFT) calculations can be performed.

3.4.2 Time-dependent density functional theory

TDDFT calculates the optical absorption of a system by starting from the ground state Kohn-Sham orbitals and applying a linear first-order time-dependent perturbation. The usage of ground state MOs avoids any problems connected to the DFT treatment of excited states. The so-called adiabatic local density approximation furthermore replaces the time dependency of the exchange–correlation functional, which allows for the employment of standard ground-state functionals, such as B3LYP. TDDFT usually provides very good excitation energies for the valence electrons, errors on the order of tenths of eV are typical. It also allows for studies of the nature of excited states which are represented by a linear combination of all singly excited Kohn-Sham orbital configurations.[42,43]

However, large underestimations of the excitation energy are normal for highly excited systems and for long-range phenomena such as distributed conjugated systems or CT transitions. The nature of a CT transition, for example an MLCT transitions in a d^6 transition metal complex, determines the error accompanied with the TDDFT calculations; a long distance between donor and acceptor results in poor, or no, interaction between the involved MO:s. As such, MLCT transitions in relatively small molecules are usually relatively well-described if hybrid functionals and large enough basis sets are used. A definitive check of the validity of the results from TDDFT calculations can be made by comparisons with experimental spectra.[42,43]

4. Charge transfer states in polymer:fullerene blends

Conjugated polymers are widely used in the field of organic electronics in, for example, solar cells, light-emitting diodes, and transistors.[44-46] Commercial products in these areas have been released on the market, but polymer-based organic solar cells have not yet reached the necessary demands in cost, stability, and efficiency.[47,48] Roll-to-roll techniques are believed to sufficiently reduce the cost by allowing high area-per-time production rates[49,50], but relevant issues regarding the efficiency and stability are still to be solved.[4,6,51] Power conversion efficiencies of ~10 % have recently been reached for solar cells produced and kept in laboratory conditions, but the efficiency for solar cell modules is still considerably lower.[52] This, together with theoretical estimates of the fundamental power conversion efficiency limit for organic solar cells to above 20 %[24], motivate further studies of the processes governing the efficiency.

The studies related to solar cells included in this dissertation (papers I-III) employ spectroscopic measurements with the aim to investigate the primary photoinduced processes occurring after the first charge transfer step in the active layer. The active layer of a plastic solar cell typically consists of a polymer and a fullerene derivative deposited on a substrate and sandwiched between two electrodes (Figure 4.1).[5,45] After light absorption (typically) in the polymer, charges are formed by charge transfer from the polymer (donor) to the fullerene (acceptor). This leads to the population of a charge transfer (CT) state consisting of the recently formed and still Coulombically bound charges.[18,53] It is the dissociation of these CT states, and to some extent their role in recombination, that has been the target of the included studies. Once the CT state has dissociated, free charge carriers are formed and can thus, in competition with charge recombination, be transported to the electrodes.

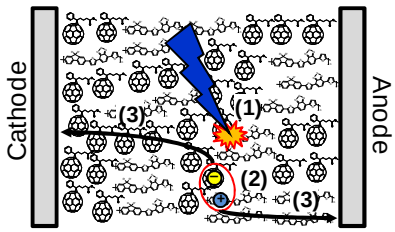

Figure 4.1. Schematic picture of an organic solar cell. (1) Light absorption in the active material leads to formation of (2) charges at the donor-acceptor interface, and these are then (3) transported within each phase to the respective electrodes.

Blending the polymer and the fullerene into a bulk heterojunction, which increases the effective interface area and decreases the average distance between donors and acceptors, has made a fast and almost 100 % efficient conversion of absorbed photons to charges feasible.[28,54,55] The bulk heterojunction has large implications for other properties of the solar cell as well, it for example sets requirements for the formation of percolation pathways to the respective electrodes for both the hole transporting (polymer) and the electron transporting (fullerene) materials. It is thus important to control the morphology of the active material in order to optimize the performance of the solar cell.[44,46,56] This can be done by varying the preparation conditions (solvent, deposition conditions, additives, etc) or by post-processing (e.g. thermal annealing). However, one inherent property when applying the bulk heterojunction concept on a polymer-based system is the development of heterogeneity along several directions: the polymer itself; the local interface between polymer-polymer, polymer-acceptor or acceptor-acceptor; phases of neat polymer or acceptor, or phases with different blending ratios of polymer and acceptor etc. It is thus indeed challenging to modify the morphology and the properties in a controlled way, the mean value of a certain property might be controllable but its heterogenic width is typically very large. This is obviously also the case for the excited state properties dealt with in this dissertation.

Another approach, in addition to the parameters mentioned above, to influence the morphology is to modify the polymer or acceptor itself. It is desirable to modify a polymer in order to reach a combination of properties in absorption, electronic structure and electronic transport that are properly balanced in order to achieve efficient light collection, charge generation and electrical transport, and to suppress charge recombination. As a result, numerous polymers and synthetic strategies have been developed during the years.[57,58,59] The systems of study in this thesis are mainly composed of blends of alternating polyfluorene (APFO) and the acceptor PCBM, see Figure 4.2. APFO polymers consist of a fluorene which is alternated by a donor-acceptor-donor segment where the donor part is a thiophene and the acceptor part is based on a benzothiadiazole. The effect of the donor-acceptor-donor segment is to modify the optical absorption towards longer wavelengths.[60]

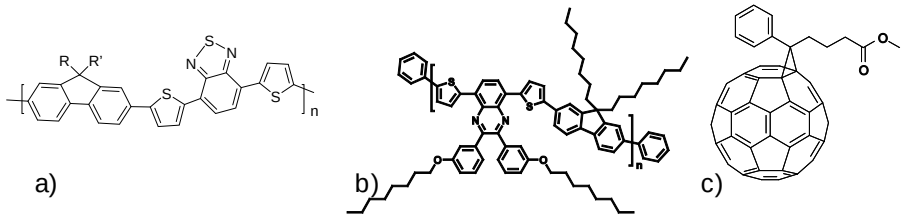

Figure 4.2. Chemical structures of the polymers studied in papers I (a), II (a and b), and III (a), and of the fullerene derivative PCBM (c).

4.1 Excited states of conjugated polymers

There are many aspects of the excited states and their properties in conjugated polymers and the purpose here is not to give a full overview. Instead, a short introduction based on a few review articles[18,28,61] will fulfill the purposes for this dissertation.

Absorption of light in a conjugated polymer leads to the formation of a Frenkel exciton, i.e. a bound (as opposed to a Wannier-Mott exciton) excited state that usually extends over several monomer units in the molecule. The exciton is formed from a J-aggregate type of interaction between the states of the individual monomers, leading to a high oscillator strength for the transition from the ground state to the lowest exciton state. The amount of delocalization over several units can be seen as a shift of the absorption and fluorescence wavelengths: larger delocalization results in more red transitions, and vice versa. (Figure 4.3) This can be observed as a blue-shift of the absorption in oligomers or monomers compared to the polymer, and can be understood by a simple particle in a box model. The formation of such chromophores in films of long polymers is believed to occur because of breaks of the conjugation due to chemical defects or large structural deformations. It is thus already here apparent that the morphology of the active layer will have an effect on the properties of the solar cell: more well-ordered films (e.g. spin cast from a "good" solvent) will, for example, allow for longer conjugation lengths and hence red-shifted spectra.

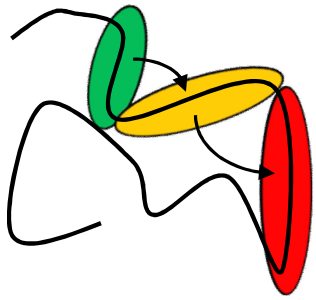

Figure 4.3. Schematic illustration of three intramolecular chromophores in a polymer chain. The arrows indicate possibilities for energy transfer.

Another characteristic feature of polymer-based films, which is due to the correlation between morphology and the formation of chromophores, is the large heterogeneity within one single film. It will lead to a manifold of excited states with different energy and a significant broadening of the absorption and fluorescence spectra. This allows for Förster energy transfer (equation 2.6) between the different chromophores, leading to a time-dependent red-shift of the fluorescence. Directly after excitation of the sample, a distribution of excited chromophores with different excited state energy will be formed (the distribution can to some extent be controlled by the choice of excitation wavelength(s)), and the sites corresponding to high energy can undergo energy transfer to nearby sites of lower energy. Downhill energy transfer is usually a very fast process, occurring on a timescale of a few ps. Energy transfer on longer timescales is thus iso-energetic and will be mediated via thermal fluctuations. Tight packing of polymer chains in films is believed to facilitate interchain energy transfer compared to intrachain energy transfer. The exciton is hence relatively free to migrate within the polymer phase, which, in terms of polymer:fullerene blends, could be required for efficient dissociation of excitons into CT states.

Transient absorption spectra of the excited states and other photoinduced species in conjugated polymers, such as charges, are usually very broad and featureless, but relatively strong. It is thus usually assumed that the transient absorption spectra in blends of polymers and fullerene derivatives, due to the weak transient absorption of fullerenes, is dominated by the polymer signal.

4.1.1 Excited states in APFO-type polymers

The absorption spectra of APFO-type polymers consist of two bands in the visible wavelength range: one around 400-450 nm and one more red-shifted. Theoretical calculations on APFO3 (poly[2,7-(9,9-dioctyl-fluorene)-alt-5,5-(4,7′-di-2-thienyl-2′,1′,3-benzothiadiazole)], Figure 4.2a) have shown that the red band corresponds

to a transition resulting in a partial charge transfer within the polymer, with the electron localized on the benzothiadiazole unit and the hole on the fluorene and thiophene units.[62] Excitation in the blue band, on the other hand, corresponds to a $\pi \rightarrow \pi^*$ transition in the conjugated backbone. The fluorescence spectra are characterized by a broad and rather featureless band with a tail extending into the red. Sometimes, a small signature of a vibrational band can be seen. Absorption and fluorescence spectra of an APFO3 film are shown in Figure 4.4.

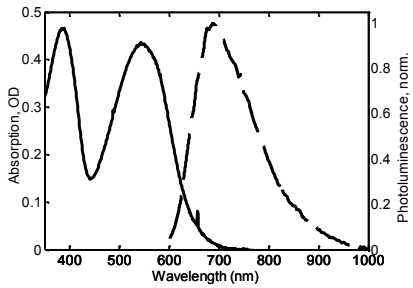

Figure 4.4. Steady-state absorption (solid line) and fluorescence (dashed line) spectra for an APFO3 film.

4.2 Photoinduced processes in polymer:fullerene blends

It is possible to generate charges in neat polymer films, but the exciton binding energy of 0.3 – 1.0 eV must first be overcome. The reason for this high exciton binding energy in neat polymers is the low dielectric constant of these types of materials, which does not allow for efficient screening of charges. However, exciton dissociation can be achieved, usually with rather low efficiency, by applying a reverse electric field or exciting with high excess energy.[28] In polymer:fullerene blends, the addition of a good electron acceptor with a LUMO level below that of the polymer significantly increases the exciton dissociation yield as the $LUMO_{polymer}$-$LUMO_{acceptor}$ difference will provide the necessary driving force for exciton breaking.

The formation of separated and extractable charges, and related challenges, in these systems has been described in detail by Clarke and Durrant[63], and only the general features and specific points relevant for the studies presented in this dissertation will be presented. A polymer exciton, which has been created at or has migrated to, the polymer:fullerene interface will in the most efficient blends undergo very fast (~100 fs) dissociation by electron transfer to the acceptor. As mentioned above, this results in a CT state, i.e. a Coulombically bound charge pair. The CT state is not

only a photoinduced product, it also has a ground state stemming from ground state interactions of the polymer and the acceptor. This leads to a, compared to the neat and blend materials, very weak and red-shifted ground state absorption and fluorescence in the blend.[64,65] More importantly, the increased distance between the electron and the hole in the CT state in comparison with the distance in the polymer exciton (leading to a lower binding energy), and the fact that the polymer and acceptor are tuned to be good hole and electron transporting materials, respectively, is believed to allow for dissociation of the CT state into mobile charges despite the low dielectric constant of the materials.

Given the high mobility of recently created charges[66,67], there is a reasonably high chance that they separate further leading to continuously lower attractive Coulomb forces and eventually to the formation of rather well-screened polarons. These can then either be extracted at the electrodes, which of course is the wanted outcome, or recombine at the polymer-fullerene interface before they reach the electrodes. One usually differentiates between recombination of two charges formed from the same absorbed photon, geminate recombination, and formed from different absorption events, non-geminate recombination. These two types of recombination will exhibit different excitation intensity dependencies – geminate recombination is independent of intensity and non-geminate recombination is dependent on intensity – and their individual contributions to the total charge recombination can thus be evaluated by measurements at varying light intensities. Charge transport and recombination is not within the scope of this dissertation but a good starting point for further information is the review of Pivrikas et al.[68]

4.2.1 Kinetics and further implications of the CT state in polymer:fullerene blends

The CT state is, as described above, believed to play an important role in the formation of charges.[53,63,69] This is illustrated in Figure 4.5 by processes **2**, exciton dissociation, and **3**, CT state dissociation. The differences in Figure 4.5a and b highlight one of the major controversies about the processes associated with the CT state: the timescale and properties of its dissociation. Figure 4.5a illustrates the case when the dissociation is competing with relaxation within the local excited state manifold of one single CT state (**5a**). Such relaxation corresponds to IC and VR (chapter 2.2), and thus require very fast (<1 ps) CT state dissociation in order for charge formation to be efficient.[70,71] Figure 4.5b, on the other hand, describes the situation when CT state dissociation mainly occurs from the relaxed CT state on significantly longer timescales[72-74], not competing with relaxation. The CT manifold then corresponds to a global manifold of heterogeneously distributed local CT states. It is this discrepancy in the role of the CT state in charge formation in polymer:fullerene blends that has motivated the studies in papers II and III.

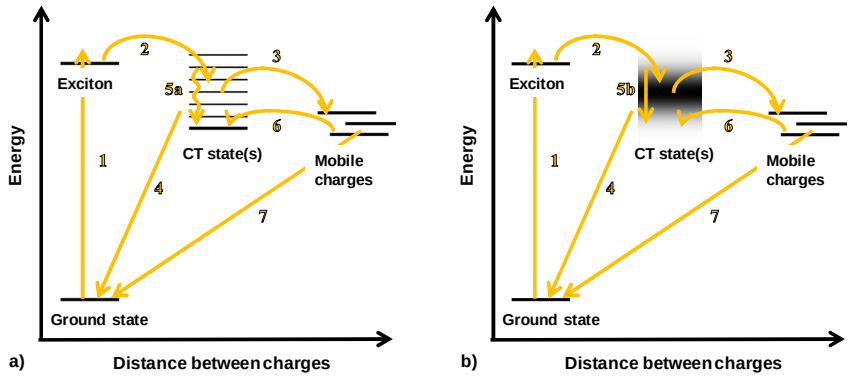

Figure 4.5. Schematic view of the processes in polymer:fullerene blends relevant for this study: 1) light absorption in the polymer, 2) dissociation of polymer excitons into the CT state manifold, 3) dissociation of the CT states into mobile and more separated charges, 4) recombination of the CT states to the ground state, 5) relaxation within the (a) local CT state manifold consisting of discrete vibronic or electronic CT state levels or (b) global CT state manifold consisting of a Gaussian distribution of CT states, 6) charge recombination to the CT state, 7) charge recombination directly to the ground state, and 8) formation of charges directly from the polymer excitons. The manifold of polymer excitons is not showed for clarity reasons.

Furthermore, electroluminescence studies have shown that charge recombination to the ground state occurs via the CT state (**6** and **4**)[75], but an additional recombination pathway directly to the ground state (**7**) cannot be excluded.[72] However, it seems as the lowest CT state indeed is the lowest available "charge type" state (i.e. not including triplet states) as its energy can be used to describe the open circuit voltage for a particular blend.[16,17] It has thus been suggested that the free charges, i.e. the polarons, are interacting with the CT states during their extraction/recombination time[76], giving rise to a quasi-equilibrium between polarons and CT states.[63] The relationship between the CT state energy and the open circuit voltage, together with the participation of the CT state in recombination, motivates further studies of its properties and the associated processes.

4.3 Paper I: the CT state manifold in APFO:fullerene blends

The main objective of paper I is to investigate the effect of driving force on charge recombination in films of APFO3:fullerene blends. Earlier spectroscopic studies[72,77] of the photoinduced processes of APFO3:PCBM blend films have resulted in the following scheme: 1) Very fast (~200 fs) dissociation of the polymer exciton into

CT states (also referred to as "bound charge pairs" in the paper) with almost 100 % efficiency. This means that no, or very little, energy transfer occurs before exciton dissociation, which is interpreted as good mixing of APFO3 and PCBM throughout the film. 2) Dissociation of the CT states into charges with a lifetime of tens of ps. 3) Geminate recombination of charges on tens and hundreds of ns (for sufficiently low excitation intensities, see Figure 4.6). Paper I expands the previous study by measurements on blends of APFO3 and the fullerenes [70]PCBM ([6,6]-phenyl-C71-butyric acid methyl ester) and [70]BTPF (3′-(3,5-bis-trifluoromethylphenyl)-1′-(4-nitrophenyl)pyrazolino[70] fullerene), which are shown to undergo the same type of processes as the blend with PCBM. The three processes are labeled in the corresponding kinetic trace of APFO3:[70]PCBM in Figure 4.6. No significant effect of the driving force on the charge recombination is observed. Instead, it is found that longer initial charge separation distances after CT state dissociation is the reason for longer charge lifetimes.

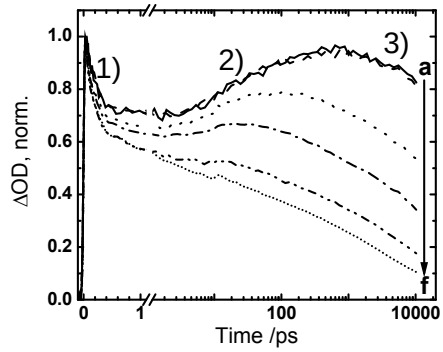

Figure 4.6. Transient absorption kinetics at 1000 nm probe wavelength for a 1:1 blend of APFO3:[70]PCBM at various excitation fluencies (increasing from a to f). The time axis is linear up to ~1 ps and logarithmic later on.

The long CT state lifetimes (up to ~6 ns) obtained from the TCSPC measurements, which is the most relevant part of paper I for the main topic of this dissertation, compared to the relatively short CT state lifetime obtained with transient absorption measurements, led us to suggest that the manifold of CT states results in large variations in lifetimes. The manifold represents a large variation in energy, which is expected to result in similarly large variations of activation barrier and/or driving force for CT state dissociation. Another important consequence of the presented results is that all observed CT state decay components are significantly longer than expected for relaxation processes, which means that the relevant CT state manifold observed in these experiments has a global nature.

Furthermore, no correlation between driving force, i.e. excess energy, and the CT state dissociation rate is observed. The blend with [70]BTPF, which corresponds to the highest driving force for charge separation (largest LUMO-LUMO differences),

give the shortest charge separation distances. This means that no positive influence of excess energy is seen for the CT state dissociation.

4.4 Paper II: transient absorption spectral signatures of CT states

Two of the three processes used to describe the photoinduced kinetics in the APFO3:fullerene blends in paper I are supported by at least two separate experimental observations. The initial fast dissociation of the polymer exciton corresponds well with the hundredfold quenching of the neat steady-state polymer emission, and the recombination at long timescales is seen at all probe wavelengths, including the ground state bleach. However, the assignment of the CT state dissociation is primarily made from a rise in kinetics when probing at ~1000 nm. It is indeed rather natural to assign a kinetic rise between the well-characterized processes of exciton dissociation and charge recombination to a process connecting these two events, i.e. to the dissociation of the CT state. But it could be a signature of other processes as well, for example spectral relaxation due to the thermalization of charges formed by very fast CT dissociation.

The main samples of study in paper II are films of the polymer APFO15 (poly[2,7-(9,9-dioctylfluorene)-alt-5,5-(5′,8′-di-2-thienyl-(2′,3′-bis-(3″-octyloxyphenyl)-quinoxaline))], Figure 4.2b) and its 1:1 blend with PCBM. This polymer is very similar to APFO3 in most regards, and also transient absorption measurements of the neat and blend films based on APFO15 show the same general behavior as the corresponding APFO3 samples. It is thus possible to use the same model of processes as for APFO3 and its PCBM blend to interpret the data. However, a clear signature of an isosbestic point in the APFO15:PCBM films, which had not been observed for the APFO3:PCBM films, provides evidence for the previously made correlation between the observed rise in kinetics and the CT state dissociation (Figure 4.7a). An isosbestic point is typically interpreted as a clear indication of a reaction between two different states (species) that occurs while the population (or concentration) of all other states is constant. The two involved states have the same oscillator strength at the isosbestic wavelength, and the conversion of one state into the other will thus not result in any intensity changes at that particular wavelength. These unique requirements for an isosbestic point means that it is very improbable for such a feature to be caused by any other type of processes. The negative ΔOD of the isosbestic point furthermore implies that the ground state cannot be one of the involved species; the isosbestic point is instead formed on top of the ground state bleach. Hence, the match in risetime at infrared probe wavelengths with the lifetime of the isosbestic point provides the support for the assignment of the CT

state dissociation process to the rise seen in kinetics on tens of ps. By pursuing further measurements, we also managed to observe a similar isosbestic point in APFO3:PCBM blends (Figure 4.7b).

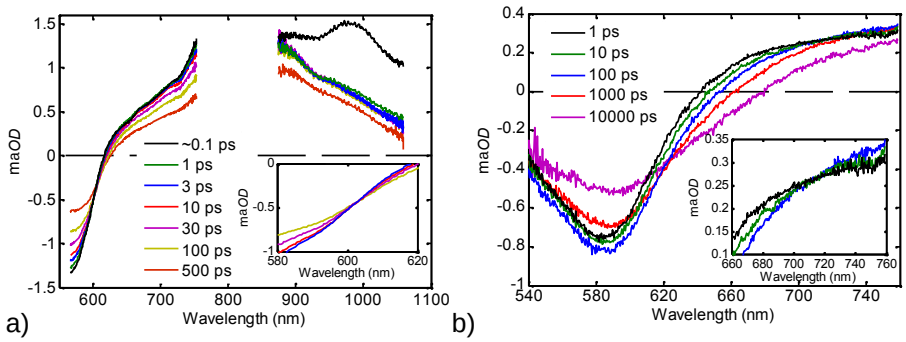

Figure 4.7. Transient absorption spectra of a) APFO15:PCBM and b) APFO3:PCBM blend samples. The observed isosbestic points are highlighted in the insets.

The definitive assignment of the CT state dissociation from relaxed CT states in these samples allows for the estimation of the minimum amount of charges that are formed via this route. This gives a minimum yield of 18 %, and it is quite probable that the actual yield is considerably higher. The contribution to charge formation from the relaxed CT states is thus significant in these type of materials. It can, on the other hand, be argued that also relaxed CT states in blends based on APFO3 and APFO15 should be considered to have excess energy for charge formation because of the high-lying LUMO levels for these polymers (0.7-0.8 eV higher than the LUMO of PCBM). However, the characteristic rise in infrared transient absorption kinetics has also been observed in blends based on polymers with much lower LUMO. Such a trace is shown in Figure 4.8 for the blend of APFO-Green9 and PCBM, which has a LUMO-LUMO difference of 0.1 eV.

Solar cells based on APFO-Green9:PCBM give a rather moderate efficiency (2.3 %) albeit the extended absorption in combination with relatively high open circuit voltage (0.81 V).[78] This suggests that the recombination losses are comparably high in these materials. If low driving force is the reason for these losses or if they are due to other effects is not clear at the moment. Most probably a combination of several factors, such as mobility and morphology, are determinant for the final efficiency. High driving force might be one general solution to overcome (or hide) many other problems, as it could lead to too fast charge separation for other processes to compete with it. The aim should thus be to lower the excess energy as much as possible but still not allow for loss processes to dominate the performance. This is certainly a balance act, where the mean values of many properties need to be perfectly matched to also account for the broad distribution that unavoidably are associated to every property of these materials because of their large heterogeneity.

In order to find the optimum balance, each step of the solar cell dynamics has to be thoroughly evaluated. From the study in paper II, it at least seems as if the CT state dissociation should not be one of the processes requiring particularly large energy losses.

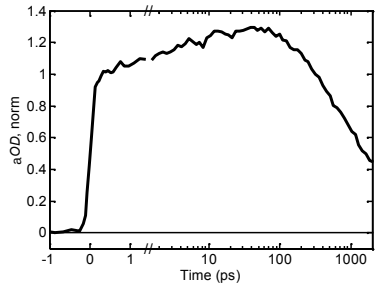

Figure 4.8. Transient absorption kinetics at 1050 nm probe of an APFO-Green9:PCBM 1:1 blend film.

4.5 Paper III: time-resolved fluorescence of short-lived CT states

Transient absorption measurements probe all excited states that have an allowed transition at a specific wavelength, which in many cases leads to a signal consisting of contributions from several different states. The obtained data thus reports on the major contributor, determined by the product of the population and oscillator strength of each state at a particular wavelength and time. Fluorescence measurements, on the other hand, only report on the emitting states, such as the CT state, whereas dark states, such as charges, will have no contribution at all. This makes fluorescence a very powerful tool which can be employed to obtain clear signals from excited states with low population.

Earlier fluorescence studies have, similarly to paper I, reported typical CT state lifetimes on the order of a few hundred ps to a few ns.[65,76,79] However, the CT state fluorescence decay should also contain a component with a lifetime of a few ps if the assignment of the CT state in paper II is correct. In order to confirm this and to use a, presumably, more sensitive probe of the CT state, time-resolved streak camera fluorescence measurements were performed on films and devices of both neat APFO3 and the APFO3:PCBM 1:4 blend. This is the blend that gives the highest solar cell efficiency (3.5%).[80] The low emission intensity of the CT state was compensated by increasing the slits of the streak camera, at the expense of time resolution (~10 ps).

Very fast quenching of the polymer exciton is, as expected, observed at early times for the APFO3:PCBM samples. After the response-limited exciton decay, the spectra show a clear indication of a CT state band centered around 820 nm. Spectra at longer times can be completely described by emission from CT states. Kinetic traces averaged over the CT state band for both films and devices at different electric field conditions are shown in Figure 4.9a, whereas Figure 4.9b reports on the integrated area under each trace from ~20 ps and onwards as a function of applied voltage. The exponential decrease of integrated intensity with applied reverse bias for these times clearly indicates that this wavelength and time region is dominated by CT state emission. The traces in Figure 4.9a furthermore reveal two different time regimes for the electric field influence: early-time kinetics is significantly less sensitive to weak fields (open and short circuit) than the kinetics at longer times. This led us to model the film data with two types of CT states, one that is formed by exciton dissociation and that rapidly (tens of ps) dissociates further into charges, and one that is formed through recombination from close-lying charges that have not dissociated far enough to undergo spin mixing. These charges are still less coupled than charges in a CT state and they should thus be more sensitive to the effect of an electric field. Another possible explanation is to consider the differences in electric field dependence as an effect of the manifold of CT states stemming from sample heterogeneity. The long-lived CT states would then correspond to low-lying states not particularly prone to dissociation, which thus are significantly affected by the electric field. Most likely both of these effects are present, it is for example quite plausible that the recombination of charges into the CT state mostly occurs to a low-energy state at the bottom of the CT state manifold.

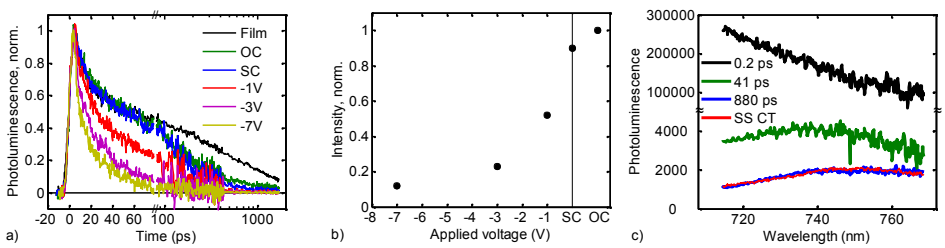

Figure 4.9. a) Kinetic traces for APFO:PCBM 1:4 films and devices averaged at the CT state emission at different electric field conditions. b) Integrated intensities of the traces in a) from ~20 ps and onwards as a function of applied bias. c) Decay associated spectra and lifetimes (legend) obtained from fitting of the blend film. A steady-state spectrum is also included (red). Note the break of the time axis and the intensity axis in a) and c), respectively.

Decay associated spectra from the fitting of the APFO3:PCBM 1:4 film are shown in Figure 4.9c. Totally four components were used in the fitting; two consecutive steps that end up in a state characterized by biexponential decay kinetics. A TCSPC

trace measured at 825 nm was also included in order to properly describe the long components with a major contribution on timescales longer than the maximum 2 ns of the streak camera. The first component corresponds to the dissociation of polymer excitons into CT states, and it was thus locked to the lifetime obtained from transient absorption measurements (200 fs). Its associated spectrum matches the early time streak camera spectrum of a neat APFO3 film, which is as expected. The second component should then correspond to the dissociation of CT states into charges, and both its spectrum and lifetime are supporting this view. Transient absorption measurements have resulted in a CT state lifetime of 50 ps for the 1:4 blend[72], which is in very good agreement with the 41 ps obtained in this study. However, the decay associated spectrum has a contribution in the blue part that deviates from the steady-state spectrum of the blend, tentatively ascribed to either emission from energetically high-lying CT states in the CT state manifold or rest polymer (or PCBM) emission. The last two components were assumed to have the same spectrum and the resulting biexponential decay (with characteristic lifetimes of 880 ps and 4.6 ns) could be explained either by an equilibrium between charges and CT states or as a multi-exponential charge recombination process. The spectrum agrees very well with the steady-state spectrum of the blend, which is dominated by CT state emission. However, these two lifetimes do, in contrast to the first two components, not match the transient absorption data very well. Transient absorption measurements show a main recombination rate of 30 ns, which is one order of magnitude higher than obtained in the present study. It is thus clear that the two long components do not describe the recombination of a majority of the charges, but rather a subpopulation giving rise to the emission on the timescales covered in this study.

In summary, a very good agreement of the polymer exciton and the CT state dissociation was found between time-resolved fluorescence and transient absorption measurements. Time-resolved fluorescence experiments with high temporal resolution is shown to give a clear CT state signal, and can thus be used as a powerful tool in future investigations of the charge formation process in plastic solar cells.

4.6 Conclusions and future outlook

Based on the studies included in this dissertation, we assign the previously proposed charge separation process in APFO-type polymers blended with fullerene derivatives to dissociation of the CT state. This assignment is derived from the observation of isosbestic points in transient absorption together with the CT state fluorescence decay on similar timescales as the previously reported charge separation. Hence,

further evaluation of the importance of the CT state in the charge formation process is feasible. It is, for example, estimated that a significant part of all charges (~20 % or more) have to be formed via the CT state.

More importantly, the timescale of the observed CT state dissociation is much slower than typical times associated with relaxation processes (VR and IC) in polymers. A significant part of all charge carriers is thus formed through relaxed CT states, without any need for excess driving force from high-lying CT states.

It is obviously possible, and actually rather probable, that the CT state dissociation in different (types of) materials could be significantly different than in the here studied blends based on APFO-type polymers; differences in relative energies of polymer, fullerene and CT states, morphology, polymer-PCBM interaction, charge mobility etc. should influence the need for excess energy. In this context, the studies included in this dissertation point towards future strategies to develop efficient solar cell materials without large amount of excess energy. The extra few hundreds of meV, otherwise lost in the charge formation process, would then instead contribute to the efficiency of the cell.[24,81]

The presented studies also represent two experimental methodologies that evidently can be used to evaluate the dissociation of relaxed CT states into charges, which is necessary if future comparative studies of different materials are to be carried out. Transient absorption measurements on polymer:fullerene blends require low excitation intensities because of the high influence of non-geminate recombination at elevated intensities. It is also valuable to cover both shorter (fs) and longer (ns) timescales in order to avoid misinterpretation of data stemming from different contributions to the transient absorption signal. Time-resolved fluorescence experiments need to be sensitive enough to the low CT state emission quantum yield and still provide a sufficient time resolution to capture processes on a few tens of ps. None of these experimental conditions are easily realized, but a carefully prepared study of different materials with various properties could still be rewarding in terms of the insights gained on the CT state dissociation and its dependence on excess energy.

5. Excited state properties of Ru^{II}-polypyridyl complexes

Transition metal complexes, such as Ru^{II}-polypyridyl complexes, can be used in a wide range of applications, for example photonics, molecular electronics and medicinal inorganic chemistry.[82-84] Particularly d^6 complexes, based on metals from groups 6-9, have shown promising properties towards photoinduced applications, including light harvesting systems.[84] Among the d^6 complexes, Ru^{II}-polypyridyl complexes stand out as the prototypical systems of study because of their favorable physical properties, such as high chemical stability, reversible redox properties, strong emission, and long excited-state lifetime.[19] As a result, Ru^{II}-polypyridyl complexes are probably the most thoroughly investigated transition metal complexes today and they hence serve as excellent model systems in many studies. Insights on the excited state properties, in particular the connection between room-temperature lifetime and structure, gained in these studies are not only valuable for the fundamental understanding of transition metal complexes, but also provide information that can be used for developing successful synthetic strategies. These could eventually be applied to the synthesis of complexes based on more abundant and easily accessible d^6 metal centers.

The motivation for the studies on the Ru^{II}-polypyridyl complexes included in this dissertation (paper IV-VI) is artificial photosynthesis. Artificial photosynthesis aims to mimic and improve the natural photosynthesis in order to convert sunlight into a usable form of energy.[13,27] One approach for directional energy or electron transfer is to construct covalently bound DPA macromolecules.[19,27,85-87] A vectorial alignment of the three DPA moieties (Figure 1.1) is required in order to obtain the preferential directionality in the transfer process. Therefore, bis-tridentate ligands, which easily can provide directionality via substitution along the pseudo-C_2 axis, are preferable as photosensitizers compared to the more well-characterized tris-bidentate complexes which result in isomeric reaction mixtures when used as building blocks in polymolecular systems (Figure 5.1). However, as described below, the introduction of bis-tridentate ligands can easily lead to deterioration of the excited state properties that are crucial for efficient and repeated light harvesting in the DPA arrays.

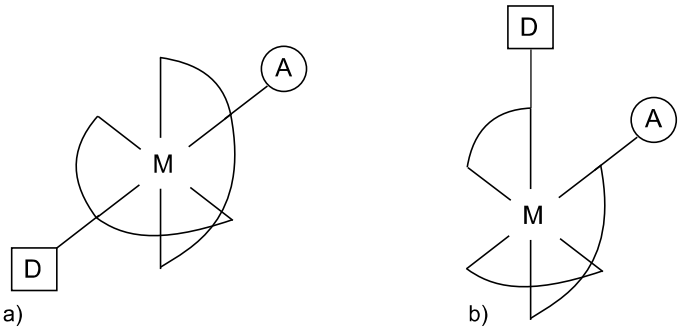

Figure 5.1. Illustration of a linear DPA array obtained by substituting D and A moieties on a) a bis-tridentate transition metal complex with the central metal M and b) one possible isomer when using a tris-bidentate complex instead.

Quantum chemical calculations coupled to kinetic experiments allow for evaluations of the underlying causes for the unwanted changes in excited state properties, and in particular DFT calculations have been shown to provide reliable and important insights into these type of questions related to transition metal complexes.[31,32,33] We have thus employed DFT and TDDFT calculations to study the ground and excited state properties of the bis-tridentate complexes shown in Figure 5.2 with the specific aim to investigate how to increase the room-temperature lifetime without reducing other qualities of the complex. This was achieved by expanding the initial calculations at the optimized geometries by calculating PESs for relevant deactivation pathways. Before presenting the results from these studies, a short summary of the electronically excited states in Ru^{II}-polypyridyl complexes will be given.

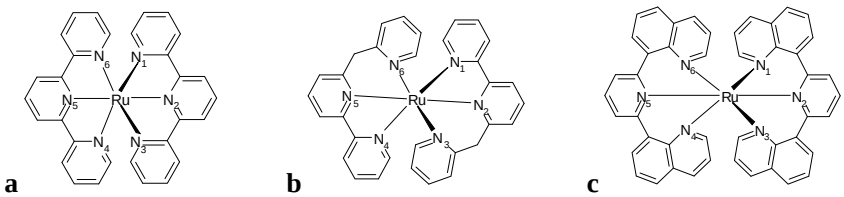

Figure 5.2. Chemical structures of the complexes studied in paper IV (c), V (a, b, and c), and VI (a and c).

5.1 Excited states of Ru^{II}-polypyridyl complexes

A schematic picture of the electronic states of Ru^{II}-polypyridyl complexes that are involved when exciting into the lowest absorption band is shown in Figure 5.3. Excitation corresponds to d → π* transitions resulting in a ^{1}MLCT state, and is followed by very rapid (within 1 ps) ISC to the ^{3}MLCT state. The rapid crossing is

mediated by the presence of the heavy Ru^{II} ion, which is believed to couple the two states and thus create a direct relaxation channel for the ISC.[88] The ^{3}MLCT state is thus the starting point for subsequent electron or energy transfer processes in molecular assemblies, and a long ^{3}MLCT lifetime is therefore desirable. There are two pathways that lead to depopulation, and hence govern the lifetime, of the ^{3}MLCT state: direct transitions to the ground state or thermally activated processes to other excited states. Direct transitions to the ground state occurs both radiatively (phosphorescence) and non-radiatively (ISC) whereas activated processes usually proceed via the ^{3}MC state. The ^{3}MC state is formed when the excited π^* electron is transferred into an empty e_g orbital (see Figure 5.4), and it is this ^{3}MLCT-^{3}MC conversion that is believed to limit the room-temperature lifetime of many Ru^{II}-polypyridyl complexes. It has furthermore been proposed that an equilibrium between the ^{3}MLCT state and the ^{3}MC state sometimes develops during the evolution of the excited state population.[19,89]

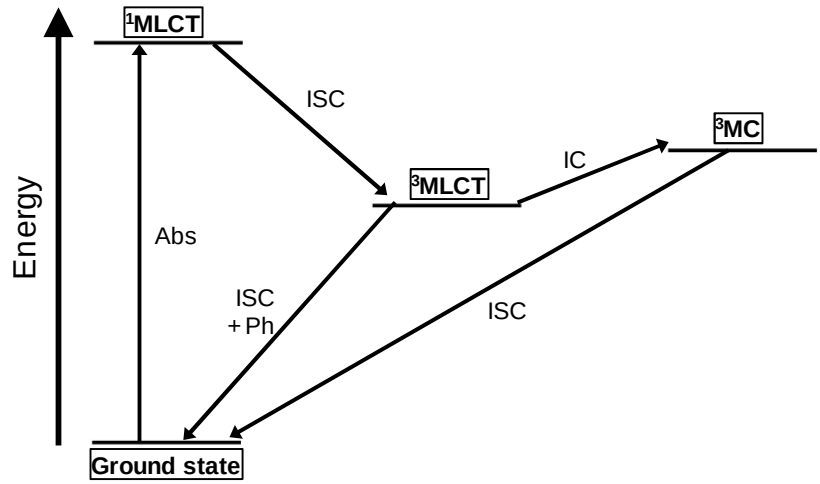

Figure 5.3. A Jablonski diagram illustrating the most important states and photoinduced processes in Ru^{II}-polypyridyl complexes. Most experimental lifetime studies do not consider the ^{1}MLCT-^{3}MLCT transition as most of the photophysical processes occur from the ^{3}MLCT state.

5.1.1 Ligand field theory

The energy of the ^{3}MC states in (close to) octahedral transition metal complexes is coupled to the energy of the d_{z^2} and $d_{x^2-y^2}$ orbitals. The energy difference between the ^{3}MLCT and ^{3}MC states can thus be understood in terms of ligand field theory, which describes the splitting of the metal d orbitals upon coordination of ligands. Figure 5.4 illustrates how the five degenerate d orbitals of an uncoordinated metal are split into two levels when interacting with the ligands: one of t_{2g} symmetry

consisting of the d_{xy}, d_{xz} and d_{yz} orbitals and one of e_g symmetry consisting of the d_{z^2} and $d_{x^2-y^2}$ orbitals.

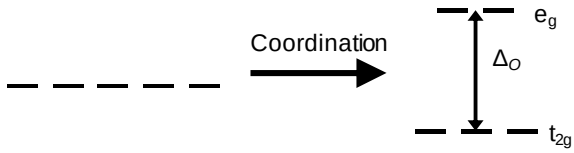

Figure 5.4. Illustration of the ligand field splitting of the degenerate five d orbitals of a transition metal when changing conditions from a completely symmetric field to an octahedral field created from the coordination of ligands.

The magnitude of the ligand field splitting, Δ_O, depends on three factors: 1) the electrostatic field from the ligands, 2) the σ-bonding with the ligands, and 3) the π-bonding with the ligands. An increased interaction between the metal and the ligands, for example via an enhanced octahedral geometry, results in a higher electrostatic field and larger splitting, hence leading to up-shifted ^{3}MC states.[90]

In summary, ligand field theory provides guidance on synthetic strategies to prolong the ^{3}MLCT state lifetime for complexes where it is limited by activated decay via the ^{3}MC state.

5.1.2 Analysis of experimental kinetics

The emissive nature of the ^{3}MCLT state allows for experimental studies of the excited state kinetics of Ru^{II}-polypyridyl complexes by time-resolved photoluminescence techniques.[89] Typically, a single-exponential decay corresponding to a first order reaction (equation 2.1) is obtained in solution. Information about the decay channels is acquired by measuring the temperature dependence of the phosphorescence and applying a phenomenological model using the Arrhenius' equation (equation 2.2) to fit the data. One or more Arrhenius' terms are included, depending on, for example, the measured temperature range. Measurements from 77 K to room temperature usually include two Arrhenius' terms, one to account for the thermal equilibrium of the three degenerate states that actually constitute the ^{3}MLCT state (remember the three t_{2g} orbitals in Figure 5.4) and one corresponding to the activated decay of the ^{3}MLCT state via the ^{3}MC state. Usually the second term dictates the room-temperature lifetime, and the focus is thus to on its kinetics which is analyzed with the following model:

$^3\text{MLCT} \rightarrow {}^3\text{MC}$ rate constant = k_a (5.1)

$^3\text{MC} \rightarrow {}^3\text{MLCT}$ rate constant = k_b (5.2)

$^3\text{MC} \rightarrow \text{GS}$ rate constant = k_c (5.3)

which gives the following expression for the observed rate:

$$k = k_a \cdot (k_c/(k_b + k_c)) \quad (5.4)$$

if steady-state conditions are assumed for the ^{3}MC state.[85]

There are two limiting cases for equation 5.4. If $k_c >> k_b$, the observed rate will be equal to k_a. This corresponds to irreversible ^{3}MLCT–^{3}MC state crossing followed by a fast recovery of the ground state. If instead $k_b >> k_c$, the ^{3}MLCT and ^{3}MC states are in equilibrium and equation 5.4 turn into:

$$k = k_a \cdot (k_c/k_b) = k_c \cdot K \quad (5.5)$$

where K is the equilibrium constant. As known from chemical kinetics:

$$K = \exp(-\Delta H/RT) \cdot \exp(\Delta S/R) \quad (5.6)$$

where ΔH and ΔS are the enthalpy and the entropy differences between the ^{3}MLCT and ^{3}MC states, respectively. However, it has usually been assumed that the entropy difference is sufficiently small to neglect the entropic term.[89]

The obtained Arrhenius' pre-exponential factor, A (equation 2.2), is believed to carry information about which of the abovementioned limiting cases is dominating. For the first case ($k_c >> k_b$), A corresponds to a typical vibrational frequency and should be on the order of 10^{12}-10^{14} s^{-1}. Lower values of A has also been observed and has led to more complex interpretations, sometimes even involving additional excited states, coupled to the second case ($k_b >> k_c$) described above.

5.2 Lifetimes of bis-tridentate Ru^{II}-polypyridyl complexes

The model complex among bis-tridentate polypyridyl Ru^{II}-complexes is $[Ru^{II}(tpy)_2]^{2+}$ (Figure 5.2a, tpy is 2,2′:6′,2″-terpyridine). However, this complex has too short room-temperature excited state lifetime (250 ps)[91] to be used as, for example, a photosensitizer in DPA arrays. The short lifetime is due to fast activated decay through the ^{3}MC state stemming from a low energy gap between the ^{3}MLCT and the ^{3}MC states because of a small ligand field splitting.[85,92] The weaker ligand-field splitting compared to tris-bidentate complexes is in turn believed to originate from higher steric strain of the ligand resulting in a less octahedral coordination.[92] Deactivation of $[Ru^{II}(tpy)_2]^{2+}$ is assumed to belong to the limiting kinetic case where the ^{3}MC state rapidly decays back to the ground state, i.e. where $k_c >> k_b$ and the observed rate constant is equal to k_a.[85] The obtained pre-exponential factor ($1.9 \cdot 10^{13}$ s^{-1})[91] supports such an assignment.

Various strategies to increase the room-temperature lifetime by increasing the ^{3}MLCT-^{3}MC energy gap, and thus slow down the activated decay route, of bis-tridentate polypyridyl Ru^{II}-complexes have been explored[92], but many of them also lead to a stabilization of the ^{3}MLCT state energy. This reduces the driving force for further reactions and can thus prohibit the desired function of the molecular assembly. However, an increased octahedral coordination should, according to ligand field theory, increase the ligand field splitting without influencing the ^{3}MLCT state energy. A project with the specific aim to increase the room-temperature lifetime of bis-tridentate polypyridyl Ru^{II}-complexes by introducing ligands with larger bite angles, and thus allowing for a more octahedral coordination, led to the successful development of complexes with increasingly longer lifetimes.[14,93-95] Paper IV reports on the most long-lived complex among these, which displayed a μs room-temperature lifetime.[96] Similar lifetimes have since been achieved using the same strategy[97] or by introducing a strongly σ-donating and weakly π-accepting tridentate carbene ligand.[98]

5.3 Paper IV: the first bis-tridentate Ru^{II}-polypyridyl complex with a μs lifetime

This paper describes the successful development of a bis-tridentate polypyridyl Ru^{II}-complexes with a room-temperature lifetime of 3 μs, $[Ru^{II}(dqp)_2]^{2+}$ (Figure 5.2c, dqp is 2,6-di(quinolin-8-yl)pyridine). It also features all required properties for a good photosensitizer, including high stability, strong absorption, and high ^{3}MLCT state energy.

DFT and TDDFT calculations of the geometry and the excited state properties were performed before the successful synthesis of $[Ru^{II}(dqp)_2]^{2+}$. These showed an almost perfect octahedral coordination, up-shifted e_g levels, an energetically suitable lowest absorption band dominated by ^{3}MLCT transitions, Ru-centered HOMO to HOMO-2 corresponding to the three t_{2g} orbitals, and a well-delocalized LUMO covering both ligands (Figure 5.5). Geometry optimizations of the lowest triplet state furthermore confirmed that it was of ^{3}MLCT nature, where an electron has been promoted from a ground state d orbital to a π^* orbital of the ligands. The calculations thus suggested that $[Ru^{II}(dqp)_2]^{2+}$ would be a strong candidate for a long-lived bis-tridentate complex. All the predicted properties, including the helical arrangement of the ligands, agreed well with the experimental results, leading to the long room-temperature ^{3}MLCT state lifetime. The long lifetime and the significant density of the LUMO at the C4 position of the central pyridine are both promising properties for vectorial electron transfer in DPA arrays, and $[Ru^{II}(dqp)_2]^{2+}$ has also experimentally been shown to be useful for such purposes.[15]

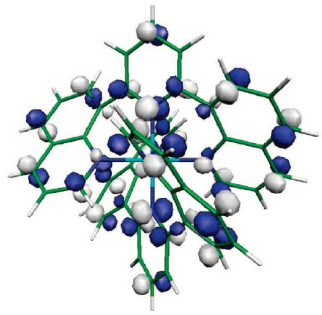

Figure 5.5. LUMO of $[Ru^{II}(dqp)_2]^{2+}$ obtained from the DFT calculations performed in paper IV.

5.4 Paper V: potential energy surfaces of the lowest excited state predict trends in ^{3}MLCT lifetimes

Examples of other successful strategies to achieve long room-temperature lifetimes[98], and of bis-tridentate Ru^{II}-polypyridyl complexes with short ^{3}MLCT lifetimes despite an octahedral geometry[99] suggest that the properties calculated at the ground and ^{3}MLCT state geometries are not sufficient to predict the ^{3}MLCT state room-temperature lifetime. Comparative DFT calculations on $[Ru^{II}(dqp)_2]^{2+}$ and other selected Ru^{II}-polypyridyl complexes have indeed shown that the calculations in paper IV, albeit the seemingly good predicting power, did not provide conclusive evidence of a long ^{3}MLCT state lifetime.[100] A first step towards improved predictive power would be to also characterize the ^{3}MC state. Calculations show that the ^{3}MC state minimum is shifted to longer Ru-N bond lengths compared to the ^{3}MLCT state minimum.[101,102] This means that the lowest triplet state for a given geometry will correspond to the ^{3}MLCT state for short Ru-N bond lengths and the ^{3}MC state for long Ru-N bond lengths. The ^{3}MC state will thus be the lowest triplet state around its energy minimum, which allows for the utilization of the variational principle when performing geometry optimizations of the ^{3}MC state. By employing this strategy, which has also been used in calculations on other d^6 complexes (see e.g. reference 103), it is possible to shed some additional light on, for example, the difference in ^{3}MLCT-^{3}MC state energy.[100-102,104-106]

The calculations of the ^{3}MC state properties undoubtedly provides important information for the understanding of the excited state processes of the Ru^{II}-polypyridyl complexes, but they still do not allow for reliable theoretical predictions of the ^{3}MLCT lifetime.[100] Attempts to further increase the accuracy of the predictions have included calculations of one-dimensional reaction coordinate diagrams to capture the energy barrier for the ^{3}MLCT-^{3}MC state transition for several Ru^{II}-polypyridyl complexes.[107-111] In paper V, as well as in other studies[112,113],

this approach is expanded into a two-dimensional picture in order to achieve an even more complete picture. Paper V thus investigates the lowest triplet PESs along selected Ru-N coordinates for three compounds: $[Ru^{II}(dqp)_2]^{2+}$ with a long lifetime, $[Ru^{II}(tpy)_2]^{2+}$ with a short lifetime, and $[Ru^{II}(bmp)_2]^{2+}$ (bmp is 6-(2-picolyl)-2,2′-bipyridine, Figure 5.2b) with an intermediate lifetime of 15 ns.[93] The obtained PESs are shown in Figure 5.6. The scanning dimensions were selected by noting that the ^{3}MC state minima are typically characterized by the elongation of the Ru-N bonds of one ligand. PESs calculations were thus conducted by stepwise changes of one or both terminal Ru-N bonds of one of the ligands, see paper V for full details on the choice of reaction coordinates.

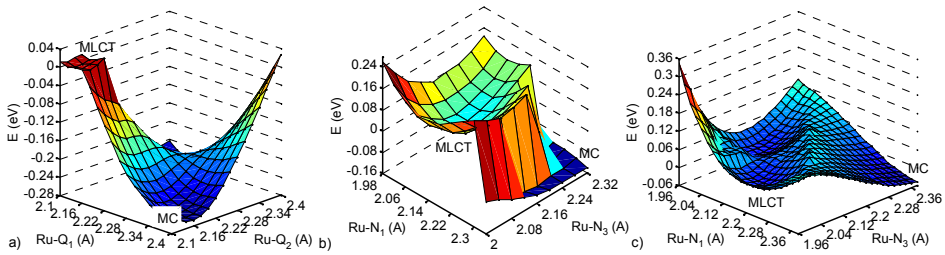

Figure 5.6. T1 PESs of a) $[Ru^{II}(tpy)_2]^{2+}$, b) $[Ru^{II}(bmp)_2]^{2+}$, and c) $[Ru^{II}(dqp)_2]^{2+}$ obtained from the DFT calculations performed in paper V.

The PESs for the three complexes show distinct differences in activation barriers for the ^{3}MLCT-^{3}MC state crossing. We furthermore note that the ^{3}MLCT and ^{3}MC state minima are characterized by regions formed in the vicinity of the actual minimum energy point. These regions correspond to a coordinate space which allows for a certain amount of vibrational degrees of freedom within the given state. It thus becomes relevant to consider the formation of ^{3}MLCT and ^{3}MC volumes on the PESs: a larger volume means that stronger or a larger amount of vibrations are required before the transition to another state will occur. This could correspond to differences in entropy and will thus become relevant when considering the ^{3}MLCT-^{3}MC deactivation pathway, something that has not been considered before.[89] The distinct observed differences in activation barrier for the three studied complexes are matched by differences in ^{3}MLCT volume; $[Ru^{II}(dqp)_2]^{2+}$ has the largest ^{3}MLCT volume and the highest ^{3}MLCT-^{3}MC state activation barrier whereas $[Ru^{II}(tpy)_2]^{2+}$ has the smallest volume and lowest barrier. These differences follow the trend in lifetime, higher barrier and larger volume results in a longer room-temperature lifetime, and might hence be good indicators of relative room-temperature lifetimes. It is thus tempting to state that these type of calculations now can serve as an effective screening tool of the ^{3}MLCT state lifetime. However, this is a limited study of three complexes and further benchmarking on other types of complexes would be useful to confirm the broader validity of this approach. It should also be

noted that the scans presented here are relatively computationally demanding: each surface is constructed from about one hundred constrained open-shell geometry optimizations.

As stated above, the large differences in the ^{3}MLCT state volume for the three complexes allows for vibrational degrees of freedom that do not lead to ^{3}MLCT-^{3}MC state crossing, and should therefore affect the entropy of the ^{3}MLCT state. This could be one of the factors governing the obtained value for the pre-exponential factor, *A*, from the fitting of temperature-dependent emission data as described above. Furthermore, the flat appearance of the ^{3}MC state volume suggests that it should be associated with correspondingly higher entropy.

The factors determining the size of the ^{3}MLCT volume can be understood as shifts of the relative position of the ^{3}MC state position in terms of energy and reaction coordinates compared to the ^{3}MLCT state. Figure 5.7 tries to capture and explain this effect using a one-dimensional picture. Short-lived complexes are here described by the ^3MC_a state surface and suffer from a low energy barrier for the ^{3}MLCT-^{3}MC state crossing, a low ^{3}MC state energy and a small ^{3}MLCT state volume, whereas long-lived complexes are described by the shifted ^3MC_b state surface with a larger energy barrier, a higher ^{3}MC state energy and a larger ^{3}MLCT state volume. A shift in either energy or reaction coordinate also results in similar changes, but the effect is enhanced if both parameters are changed.

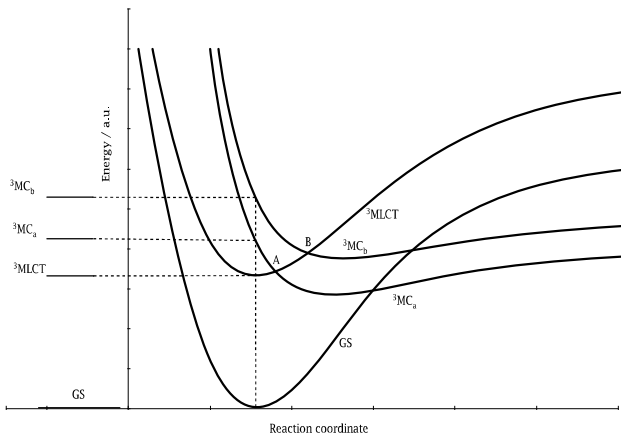

Figure 5.7. Schematic illustration of the relation between the ligand field splitting at the ground state (GS) geometry (left) and thermally activated ^{3}MLCT-^{3}MC deactivation along an effective reaction coordinate Q (right) based on the results obtained in paper V.

5.5 Paper VI: potential energy surfaces of higher-lying excited states

The PESs obtained in paper V opened up for further investigations of higher excited states than T1 by performing TDDFT calculations on the optimized T1 geometries. This is studied in paper VI, and PESs of S0, T1 and S1 for $[Ru^{II}(tpy)_2]^{2+}$ and $[Ru^{II}(dqp)_2]^{2+}$ are shown in Figure 5.8. In comparison to the study in paper V, the TDDFT approach provides information on the accessibility of the excited states at a given energy and a set of PES coordinates. For example, it provides information on which singlet states that can be excited using a certain excitation energy and which other states are available during the subsequent relaxation processes. The employed calculations do, however, not include spin-orbit coupling, which can be significant in the presence of a heavy transition metal atoms and thus introduce errors in the obtained energies and the true multiplicity.

Given the accuracy of the employed TDDFT method, it can be concluded that the energy difference between the T1 PES and other excited state PESs is too large within the region that corresponds to activated decay of the ^{3}MLCT state to allow for the involvement of any other state in the ^{3}MLCT-^{3}MC decay. Instead, the picture given in paper V (Figure 5.6) is strengthened by an even further shift of the ^{3}MC state to longer coordinates, resulting in larger activation barriers for the ^{3}MLCT-^{3}MC state crossing and larger ^{3}MLCT state volumes. The relative differences in both activation energy and ^{3}MLCT state volume between the two complexes are enhanced, which supports the large differences in room-temperature lifetimes. Moreover, the calculated activation energies (0.08 eV for $[Ru^{II}(tpy)_2]^{2+}$ and 0.25 eV for $[Ru^{II}(dqp)_2]^{2+}$) are close to the experimentally obtained values, especially for $[Ru^{II}(dqp)_2]^{2+}$.

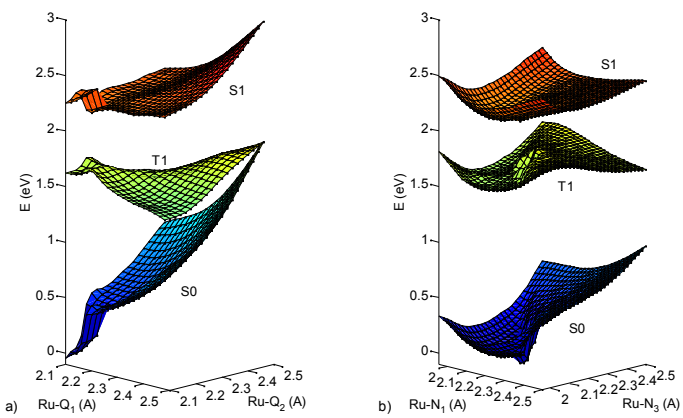

Figure 5.8. Calculated ground state (S0), T1 and S1 PESs for a) $[Ru^{II}(tpy)_2]^{2+}$ and b) $[Ru^{II}(dqp)_2]^{2+}$.

5.6 Correlating PES calculations with experimental kinetics

To this date, and to the best of my knowledge, there is no solid direct observation of the ^{3}MC state in any Ru^{II}-polypyridyl complex by any experimental technique. This suggests that no significant population is created in the ^{3}MC state during the excited state lifetime, either due to very fast decay directly to the ground state via the k_c channel (process 5.3) or because of a fast equilibrium between the ^{3}MC and ^{3}MLCT states (processes 5.1 and 5.2) that is extensively shifted towards the ^{3}MLCT state, i.e. where $k_b >> k_a$. Both these cases justify the steady-state approximation introduced in equation 5.4. This is also supported by the calculated shape of the ^{3}MC state in paper V; its shallow nature in combination with the ground state crossing seam suggest that it should undergo very fast ISC to the ground state. However, a recent study on $[Ru^{II}(tpy)_2]^{2+}$ using ultra-fast transient absorption measurements report on a biexponential excited state evolution of the ^{3}MLCT state population.[114] Such kinetics would be expected in the case of a ^{3}MLCT-^{3}MC state equilibrium[115], and they employ a pre-equilibrium approximation of the model described in chapter 5.1 to extract a value for the rate constant, K, of 0.17. Two consequences have to follow from such a high equilibrium constant. Firstly, it is not in accordance with the low energy of the ^{3}MC state compared to the ^{3}MLCT state obtained from DFT calculations. Secondly, it does not allow for the introduction of the steady-state approximation in equation 5.4. Therefore, it might be rewarding to consider the integrated rate equations.

5.6.1 Integrated rate equations

Exact integrated rate equations for reaction systems similar to the one described in chapter 5.1.2 have for example been derived in reference 116. Using a starting condition where the whole excited state population is in the ^{3}MLCT state, which is valid because of the very fast ^{1}MLCT-^{3}MLCT state conversion, one obtains the following expressions:

$$[^3\mathrm{MLCT}]_t =$$

$$[^3\mathrm{MLCT}]_0/(k_1 - k_2)\cdot((k_1 - k_a - k_d)\cdot\exp(-k_2 t) + (k_a + k_d - k_2)\cdot\exp(-k_1 t)) \qquad (5.7)$$

$$[^3\mathrm{MC}]_t = k_a\cdot[^3\mathrm{MLCT}]_0/(k_1 - k_2)\cdot(\exp(-k_2 t) - \exp(-k_1 t)) \qquad (5.8)$$

where k_d is the sum of rates (radiative and non-radiative) leading to the decay of the ^{3}MLCT state to the ground state (Figure 5.9), and k_1 and k_2 are the observed rate constants. Hence, the observed rate has a biexponential nature and is the same for the ^{3}MLCT and ^{3}MC states, as is expected for a kinetic system where an

equilibrium has a central role. Difficulties to resolve both rates are expected if the experimental conditions are not optimal, for example when the time resolution of the experimental set-up is significantly longer than one of the rates. However, this should not be used to justify the steady-state approximation in equation 5.4. An analysis of the amplitudes obtained from equations 5.7 and 5.8 instead provides the opportunity to, for example, distinguish between the extreme cases when the excited state population is mainly localized to either the ^{3}MC or the ^{3}MLCT state.

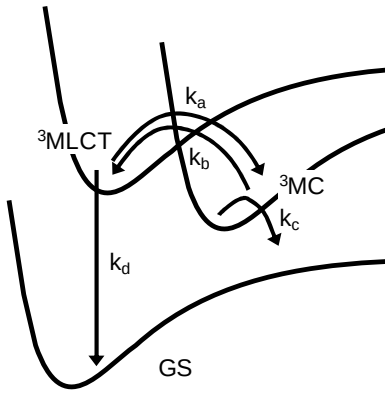

Figure 5.9. Schematic illustration of the processes associated to the excited state decay in Ru^{II}-polypyridyl complexes.

The observed rate constants in equations 5.7 and 5.8 are given by[116]:

$$k_{1,2} = ((k_a + k_b + k_c + k_d) \pm ((k_a + k_d - k_b - k_c)^2 + 4 \cdot k_a \cdot k_b)^{1/2})/2 \qquad (5.9)$$

It is still possible to evaluate the same extreme cases as for equation 5.4 in chapter 5.1.2, at least for $[Ru^{II}(tpy)_2]^{2+}$ where $k_d << k_a$, k_b, k_c under room-temperature conditions. The case when $k_c >> k_b$ results in $k_1 = k_a$ and $k_2 = k_c$, which is in relatively good accordance with the corresponding evaluation of equation 5.4 ($k_{obs} = k_a$). The "extra" rate constant, k_c, is most probably very high in most cases (~10^{10} s^{-1} or higher), but should be possible to detect if appropriate experimental measures are taken. For the opposite case when $k_b >> k_c$, one rate constant can easily be evaluated to $k_1 = k_a + k_b$, which corresponds to the equilibration rate for the ^{3}MLCT and ^{3}MC states, whereas the expression for k_2 is coupled to the decay of the states to the ground state (k_c and k_d) and is thus harder to simplify within the given assumptions. Although the clear coupling to the ^{3}MLCT-^{3}MC equilibrium, the obtained expression nonetheless is significantly different compared to the one obtained from the steady-state analysis in chapter 5.1.

It is not possible to judge whether any of the two limiting cases can be applied to the biexponential decay observed for $[Ru^{II}(tpy)_2]^{2+}$.[114] According to their pre-equilibrium analysis, k_b is approximately seven times higher than k_c. This does not

satisfy $k_b >> k_c$, but employing that limiting case one would result in similar conclusions as drawn from the pre-equilibrium analysis.

5.6.2 The kinetics of $[Ru^{II}(dqp)_2]^{2+}$

The temperature-dependent data for $[Ru^{II}(dqp)_2]^{2+}$ reveal that this is an exceptional case. A rather low activation energy (2600 cm^{-1}) is compensated by a low pre-exponential factor of $1.5 \cdot 10^{10}$ s^{-1}, resulting in the very long room-temperature lifetime. This cannot be explained solely by an increased splitting of the d orbitals introduced by the octahedral geometry, which mainly should increase the activation energy. Indeed, the finding of a non-emissive octahedral Ru^{II}-polypyridyl complex[99] points towards the importance of other factors determining the ^{3}MLCT lifetime.

The calculated PES of $[Ru^{II}(dqp)_2]^{2+}$ might offer a possible explanation of the observed behavior: the large ^{3}MLCT state volume suggests that the forward crossing rate, k_a, is small compared to $[Ru^{II}(tpy)_2]^{2+}$ and $[Ru^{II}(bmp)_2]^{2+}$ - it could be estimated to be of the same order of magnitude as k_d.[115] It is still reasonable to assume that the ^{3}MC state decay to the ground state occurs fast, meaning that the $k_c >> k_b$ case is valid. As pointed out above, this corresponds to $k_1 = k_a$ and $k_2 = k_c$ if $k_d << k_a$. However, that is not the case for $[Ru^{II}(dqp)_2]^{2+}$ and one instead obtains $k_1 = k_a + k_d$ (if $k_c >> k_a$, k_b, which is likely true). The amplitude of k_2 in equation 5.7 is $k_1 - k_a - k_d$, which in this case equals to zero. Therefore, no biexponential decay of the ^{3}MLCT state is expected. However, it is still expected for the ^{3}MC state due to the different expression of the corresponding amplitudes in equation 5.8. The obtained expression for the observed ^{3}MLCT rate in this treatment ($k_{obs} = k_1 = k_a + k_d$) explains the need to include two Arrhenius terms in the fitting of the temperature-dependent data[115] where one (k_d) corresponds to the thermal equilibrium of the degenerate ^{3}MLCT state and the other corresponds to the activated decay of the ^{3}MLCT, i.e. the k_a rate constant.

5.7 Conclusions and future outlook

The calculated PESs and their clear coupling to the room-temperature lifetime of the studied bis-tridentate Ru^{II}-polypyridyl complexes emphasize the importance to also explore the region between and around the ^{3}MLCT and ^{3}MC minima and not only the optimized geometries. It is reasonable to assume that emerging computational routes to obtain PESs which, although their need for rather time-consuming calculations, will carry enough predictive power on (relative) lifetimes to be used as screening procedures in the development of future complexes. Expansions into dynamic modeling to obtain absolute lifetimes and Arrhenius

parameters, and into similar studies of more complexes would most probably be rewarding.

In the light of the rather approximate kinetic modeling usually used to evaluate the temperature dependence of the ^{3}MLCT deactivation processes and the hope for an increase of long-lived complexes with pre-exponential factors below the typical value of ~10^{12} s^{-1}, it should also be worthwhile to reevaluate the meaning of the obtained pre-exponential factors by considering entropic contributions from the PESs and a more accurate and precise treatment of the kinetic model proposed in chapter 5.6. Furthermore, by performing accurate measurements at a wide range of temperatures it ought to be possible to find examples of clear biexponential decays, which should provide an experimental basis for the evaluation of the pre-exponential factor and the activation energy in terms of the calculated PESs.

The abovementioned measures to further extend the studies presented in this dissertation would hopefully lead to a greatly enhanced understanding of the correlation between the structure and the excited state properties of Ru^{II}-complexes. This could then be used for the development of new synthetic strategies aiming at, for example, Fe^{II}-based complexes with desirable properties as photosensitizes in DPA assemblies or other fields related to photochemistry and photophysics.

6. Final considerations

The studies presented in this dissertation aim to characterize the excited state processes in solar energy materials. One common feature of the studied systems is that a charge transfer state is of central importance in both studies: the CT state in the polymer:fullerene blends and the ^{3}MLCT state in the Ru^{II}-polypyridyl complexes. However, this similarity is to some extent of semantic character. The CT state in the blends has an intermolecular nature whereas the ^{3}MLCT state in the complexes is of intramolecular origin, which is also reflected in the different methodological approaches.

The aim of the presented investigations is ultimately to provide guidance for future development of efficient solar energy materials. DFT calculations of the lowest PES of Ru^{II}-complexes provide important insights by not only focusing on the barrier for activated ^{3}MLCT decay, but also including other factors such as vibrational degrees of freedom. It still remains to be understood how these other factors can be influenced by the chemical structure of different types of light-harvesting complexes. Once that has been achieved, it could, for example, open up possibilities to develop similar strategies for the synthesis of long-lived complexes based on other metals. Due to the high complexity of the polymer:fullerene blends, such detailed guidance is not within reach for the moment. However, it is still useful to investigate the claim for hot CT state dissociation as a necessary step for charge formation. Given that excess energy is not crucial for efficient charge formation, it seems as the development of systems that do not require excess energy is one of the most viable routes towards higher efficiency solar cells at the moment.

It is also interesting to note that the kinetic schemes for these two different states with charge transfer nature might be quite similar. The ^{3}MLCT state decay has been modeled by an equilibrium model for many years. CT states in plastic solar cells are similarly involved in an open equilibrium with charges, even though it is sensitive to the circuit definition and complicated by the heterogeneity of the polymer:fullerene blends. Therefore, the same kinetic approach as suggested to describe the Ru^{II}-polypyridyl complexes could be further developed and applied to the CT state dynamics for better understanding of its role in charge carrier generation and recombination.

Acknowledgements

First, I would like to thank my three supervisors. Arkady, for your willingness to discuss and develop the understanding of all possible aspects of things. Villy, for you passion for science and how it relates to the larger picture. Petter, for you never-ending positive spirit and encouragement. Many thanks to all of you for all exchange of ideas, interesting discussions and constant support.

Many thanks to all present and former COE members. I have appreciated the benefits of having other people in the same corridor working on similar topics. The discussions with Torbjörn deserve special acknowledgements. I am also very thankful to all non-Lund COE members and their contributions to other aspects of the polymer project, in particular Olle, Fengling, Mattias, Kristofer, Koen, Mats, Stefan, and Erdgang. Mattias, thanks for bringing floor ball to Lund!

The ruthenium studies had not been possible without the contributions from Maria and H-C, your commitment and personal interest in this project has been extremely valuable.

I also want to thank all people at Chemical physics. For laughter, discussions, Friday fikas, sports, support, and much more. The possibility to always be able to discuss scientific or practical issues with Ivan, Tönu, and Donatas have been highly appreciated. As has help with the streak camera set-up from Alice, Amal, and Annemarie. Alice, I still owe you a Monday! My present officemates, Aboma and Matthias are the best. Thank you very much for a great last year including discussions on all possible topics, and for helping me out with the thesis. I will miss you all!

The work of all administrative staff at the Chemical center is also acknowledged. Thomas and Maria, I am constantly impressed by your fast replies and actions. The old educational department and all people involved there will always be in my heart. I owe many of you my thanks, and I would like to pay special gratitude to Johan and Anita.

Finally, I thank my family and friends for all good times that have kept me floating during the tough times. I believe that Malva deserves particular recognition for this part. Without the never-ending support from my family, in particularly from Camilla during the last time, I would never have made it – I love you!

Summary in Swedish

Solenergi för alla tillfällen

Den globala energianvändningen är idag större än någonsin. Faktum är att den, i takt med världens ständiga utveckling, kommer att fortsätta öka många år framöver. Sättet som energi har producerats på historiskt används dessutom i allra högsta grad fortfarande idag och innebär daglig förbränning av stora mängder organiskt material. Detta resulterar i en ökad koncentration av växthusgaser i atmosfären, vilket i sin tur leder till en sakta ökande medeltemperatur samt alltmer dramatiska klimatförändringar. Denna utveckling är inte hållbar och därför måste förändringar ske.

Förändringar i vår energiproduktion kräver dock att det finns rimliga alternativ. Vid en uppskattning av potentialen hos olika tänkbara energislag står solenergi i en klass för sig. Ingen annan energikälla kommer i närheten av den mängd energi som når jordens yta i form av solstrålar varje dag – den totala solenergin uppgår till nästan 8000 gånger dagens totala energiförbrukningen. Det råder alltså ingen tvekan om att det bör vara möjligt att använda energin från solen för att täcka en stor del av det globala energibehovet.

Ett problem med solen som källa är emellertid att den är begränsad i sin användning, både sett över dygnet men också beroende på geografiskt läge. Den svenska vintern, vilken är den period på året då energiförbrukningen är som högst, erbjuder till exempel inte många soltimmar per dygn. Därför är det viktigt att utveckla en mängd olika tekniker för produktion och lagring av solenergi.

Denna avhandling syftar till att undersöka vad som sker när två olika typer av material för solenergi tar upp solljus. De två typerna av material motsvarar även två olika sätt att producera solenergi på. Det ena sättet bygger på plastbaserade solceller som omvandlar solljus till elektricitet. Fördelen med plastsolceller är att de har en stor potential vad gäller billig massproduktion, liten påverkan på miljön och extremt hög flexibilitet som tillåter integrering i nästan samliga produkter i vår omgivning, t.ex. elektriska apparater och kläder. En nackdel är att el är en energiform som är svår att lagra och transportera. Dessutom är det inte troligt att plastsolceller kommer att kunna tävla med stora solcellsmoduler baserade på till exempel kisel när det gäller storskalig och stationär elproduktion. I den andra delen

av de undersökningar som presenteras i avhandlingen undersöks ett intressant alternativ att istället direkt producera bränsle från solenergi. Detta sätt tar inspiration från naturen och den fotosyntes som sker i bland annat gröna växter. Fotosyntesen använder vatten, koldioxid och solljus för att skapa den energi som växten behöver för att växa. Istället för att bilda växtmassa är syftet med artificiell fotosyntes, som denna typ av solenergi heter, att producera vätgas. Vätgas har, till skillnad från de plastbaserade solcellerna, stor potential som framtida bränsle istället för olja, vilket till hög grad beror på dess goda transportmöjligheter.

Studierna på plastsolceller, vars ljuskänsliga material består av långa polymerer, undersökte egenskaperna hos de tidiga processerna efter ljusabsorption. Det är dessa processer som leder till att en elektron frigörs, vilket är det första steget för att kunna generera elektrisk ström. Med hjälp av spektroskopiska tekniker är det möjligt att studera de snabba förlopp (ner till en tusendels miljarddels sekund) som sker under dessa tidiga skeden. På så sätt kunde de relevanta tidsskalorna för de första stegen av elektronrörelse bestämmas. Samstämmiga uppgifter från olika metoder tyder på att en stor del av dessa processer inte är betydligt snabbare än den tid som behövs för att polymermaterialet ska hinna genomgå strukturell anpassning. Dessa uppgifter bidrar med relevant information för framtida vidareutveckling av material som är bättre optimerade efter de förutsättningar som gäller för varje steg i den övergripande omvandlingen av solljus till elektricitet.

Medan plastsolcellerna undersöktes experimentellt så bestod studierna som syftade till artificiell fotosyntes framför allt av teoretiska kvantkemiska beräkningar. Målet var att undersöka orsakerna till de egenskaper som de ljusabsorberande färgämnena har. Färgämnena, som ofta baseras på metallen rutenium, har till uppgift att, liksom polymeren i plastsolcellerna, ta upp ljusenergin och sedan, i form av en elektron, föra den vidare till andra delar av det komplex som utgör kärnan i artificiell fotosyntes. Studierna visade på tydliga samband mellan färgämnenas struktur och dess egenskaper relevanta för elektronöverföring. Dessa insikter öppnar upp för framtida moleklyer som effektivt kan skräddarsys för att passa in i olika sammahang. Det möjliggör förhoppningsvis också för syntes av molekyler som baseras på till exempel järn, vilket är betydligt mer lättillgängligt än det något ovanliga grundämnet rutenium.

Studierna i denna avhandling har alltså bidragit med små, men förhoppningsvis avgörande, steg mot olika typer av solenergi. Typer som förhoppningsvis kommer utgöra en del av den palett av sätt att tillgodogöra sig solenergi som vi, beroende på tillfälle, kommer att kunna välja mellan i framtiden.

References

1. Arvizu, D.; Bruckner, T.; Chum, H.; Edenhofer, O.; Estefen, S.; Faaij, A.; Fischedick, M.; Hansen, G.; Hiriart, G.; Hohmeyer, O.; Hollands, K. G. T.; Huckerby, J.; Kadner, S.; Killingtveit, Å.; Kumar, A.; Lewis, A.; Lucon, O.; Matschoss, P.; Maurice, L.; Mirza, M.; Mitchell, C.; Moomaw, W.; Moreira, J.; Nilsson, L. J.; Nyboer, J.; Pichs-Madruga, R.; Sathaye, J.; Sawin, J.; Schaeffer, R.; Schei, T.; Schlömer, S.; Seyboth, K.; Sims, R.; Sinden, G.; Sokona, Y.; von Stechow, C.; Steckel, J.; Verbruggen, A.; Wiser, R.; Yamba, F.; Zwickel, T. *Technical Summary. In IPCC Special Report on Renewable Energy Sources and Climate Change Mitigation;* Cambridge University Press: Cambridge, U.K. and New York, NY, USA, 2011.
2. Lewis, N. S.; Nocera, D. G. Powering the Planet: Chemical Challenges in Solar Energy Utilization. *Proceedings of the National Academy of Sciences of the United States of America* **2006**, *103*, 15729-15735.
3. Graetzel, M.; Janssen, R. A. J.; Mitzi, D. B.; Sargent, E. H. Materials Interface Engineering for Solution-processed Photovoltaics. *Nature* **2012**, *488*, 304-312.
4. Nielsen, T. D.; Cruickshank, C.; Foged, S.; Thorsen, J.; Krebs, F. C. Business, Market and Intellectual Property Analysis of Polymer Solar Cells. *Solar Energy Materials and Solar Cells* **2010**, *94*, 1553-1571.
5. Thompson, B. C.; Frechet, J. M. J. Organic Photovoltaics - Polymer-Fullerene Composite Solar Cells. *Angewandte Chemie-International Edition* **2008**, *47*, 58-77.
6. Brabec, C. J.; Gowrisanker, S.; Halls, J. J. M.; Laird, D.; Jia, S. J.; Williams, S. P. Polymer-Fullerene Bulk-Heterojunction Solar Cells. *Advanced Materials* **2010**, *22*, 3839-3856.
7. Marsh, R. A.; Hodgkiss, J. M., Albert-Seifried, S.; Friend, R. H. Effect of Annealing on P3HT:PCBM Charge Transfer and Nanoscale Morphology Probed by Ultrafast Spectroscopy. *Nano Letters* **2010**, *10*, 923–930.
8. Hagfeldt, A.; Boschloo, G.; Sun, L.; Kloo, L.; Pettersson, H. Dye-Sensitized Solar Cells. *Chemical Reviews* **2010**, *110*, 6595-6663.
9. Tachibana, Y.; Moser, J. E.; Gratzel, M.; Klug, D. R.; Durrant, J. R. Subpicosecond Interfacial Charge Separation in Dye-Sensitized Nanocrystalline Titanium Dioxide Films. *Journal of Physical Chemistry* **1996**, *100*, 20056-20062.
10. Benkö, G.; Kallioinen, J.; Korppi-Tommola, J. E. I.; Yartsev, A.; Sundström, V. Photoinduced Ultrafast Dye-to-semiconductor Electron Injection from

Nonthermalized and Thermalized Donor States. *Journal of the American Chemical Society* **2002**, *124*, 489-493.

11. Schnadt, J.; Brühwiler, P. A.; Patthey, L.; O'Shea, J. N.; Södergren, S.; Odelius, M.; Ahuja, R.; Karis, O.; Bässler, M.; Persson, P.; Siegbahn, H.; Lunell, S.; Mårtensson, N. Experimental Evidence for Sub-3-fs Charge Transfer from an Aromatic Adsorbate to a Semiconductor. *Nature* **2002**, *418*, 620-623.
12. Anderson, N. A.; Lian, T. Ultrafast Electron Injection from Metal Polypyridyl Complexes to Metal-Oxide Nanocrystalline Thin Films. *Coordination Chemistry Reviews* **2004**, *248*, 1231-1246.
13. Magnuson, A.; Anderlund, M.; Johansson, O.; Lindblad, P.; Lomoth, R.; Polivka, T.; Ott, S.; Stensjö, K.; Styring, S.; Sundström, V.; Hammarström, L. Biomimetic and Microbial Approaches to Solar Fuel Generation. *Accounts of Chemical Research* **2009**, *42*, 1899-1909.
14. Hammarström, L.; Johansson, O. Expanded Bite Angles in Tridentate Ligands. Improving the Photophysical Properties in Bistridentate Ru-II Polypyridine Complexes. *Coordination Chemistry Review* **2010**, *254*, 2546-2559.
15. Kumar, R.J.; Karlsson, S.; Streich, D.; Jensen, A.R.; Jager, M.; Becker, H.-C.; Bergquist, J.; Johansson, O.; Hammarström, L. Vectorial Electron Transfer in Donor-Photosensitizer-Acceptor Triads Based on Novel Bis-tridentate Ruthenium Polypyridyl Complexes. *Chemistry-A European Journal* **2010**, *16*, 2830-2842.
16. Vandewal, K.; Tvingstedt, K.; Gadisa, A.; Inganäs, O.; Manca, J. V. On the Origin of the Open-Circuit Voltage of Polymer-Fullerene Solar Cells. *Nature Materials* **2009**, *8*, 904-909.
17. Vandewal, K.; Tvingstedt, K.; Gadisa, A.; Inganäs, O.; Manca, J. V. Relating the Open-Circuit Voltage to Interface Molecular Properties of Donor:Acceptor Bulk Heterojunction Solar Cells. *Physical Review B* **2010**, *81*, 125204.
18. Bredas, J.-L.; Norton, J. E.; Cornil, J.; Coropceanu, V. Molecular Understanding of Organic Solar Cells – The Challenges. *Accounts of Chemical Research* **2009**, *42*, 1691-1699.
19. Campagna, S.; Puntoriero, F.; Nastasi, F.; Bergamini, G.; Balzani, V. Photochemistry and Photophysics of Coordination Compounds: Ruthenium. *Photochemistry and Photophysics of Coordination Compounds* **2007**, *280*, 117-214.
20. Jaffé, H. H.; Miller, A. L. The Fates of Electronic Excitation Energy. *The Journal of Chemical Education* **1966**, *43*, 469-473.
21. Jablonski, A. Efficiency of Anti-stokes Fluorescence in Dyes. *Nature* **1933**, *131*, 839-840.
22. Shockley, W.; Queisser, H.J. Detailed Balance Limit of Efficiency of p-n Junction Solar Cells. *Journal of Applied Physics* **1961**, *32*, 510-519.

23. Henry, C. H. Limiting Efficiencies of Ideal Single and Multiple Energy-Gap Terrestrial Solar-Cells. *Journal of Applied Physics* **1980**, *51*, 4494-4500.

24. Janssen, R. A. J.; Nelson, J. Factors Limiting Device Efficiency in Organic Photovoltaics. *Advanced Materials* **2013**, *25*, 1847-1858.

25. Solanki, C. S.; Beaucarnce, G. Advanced Solar Cell Concepts. *Energy for Sustainable Development* **2007**, *11, 17-23.*

26. Kasha, M. Characterization of Electronic Transitions in Complex Molecules. *Discussions of the Faraday Society* **1950**, *9*, 14-19.

27. Alstrum-Acevedo, J. H.; Brennaman, M. K.; Meyer, T. J. Chemical Approaches to Artificial Photosynthesis. 2. *Inorganic Chemistry* **2005**, *44*, 6802-6827

28. Scheblykin, I. G.; Yartsev, A.; Pullerits, T.; Gulbinas, V.; Sundström, V. Excited State snd Charge Photogeneration Dynamics in Conjugated Polymers. *Journal of Physical Chemistry B* **2007**, *111*, 6303-6321.

29. Lakowicz, J. R. *Principles of Fluorescence Spectroscopy, 3rd edition*; Springer Science+Business Media, LLC: New York, NY, USA, 2006.

30. Frisch, M. J.; Trucks, G. W.; Schlegel, H. B.; Scuseria, G. E.; Robb, M. A.; Cheeseman, J. R.; Montgomery, Jr., J. A.; Vreven, T.; Kudin, K. N.; Burant, J. C.; Millam, J. M.; Iyengar, S. S.; Tomasi, J.; Barone, V.; Mennucci, B.; Cossi, M.; Scalmani, G.; Rega, N.; Petersson, G. A.; Nakatsuji, H.; Hada, M.; Ehara, M.; Toyota, K.; Fukuda, R.; Hasegawa, J.; Ishida, M.; Nakajima, T.; Honda, Y.; Kitao, O.; Nakai, H.; Klene, M.; Li, X.; Knox, J. E.; Hratchian, H. P.; Cross, J. B.; Bakken, V.; Adamo, C.; Jaramillo, J.; Gomperts, R.; Stratmann, R. E.; Yazyev, O.; Austin, A. J.; Cammi, R.; Pomelli, C.; Ochterski, J. W.; Ayala, P. Y.; Morokuma, K.; Voth, G. A.; Salvador, P.; Dannenberg, J. J.; Zakrzewski, V. G.; Dapprich, S.; Daniels, A. D.; Strain, M. C.; Farkas, O.; Malick, D. K.; Rabuck, A. D.; Raghavachari, K.; Foresman, J. B.; Ortiz, J. V.; Cui, Q.; Baboul, A. G.; Clifford, S.; Cioslowski, J.; Stefanov, B. B.; Liu, G.; Liashenko, A.; Piskorz, P.; Komaromi, I.; Martin, R. L.; Fox, D. J.; Keith, T.; Al-Laham, M. A.; Peng, C. Y.; Nanayakkara, A.; Challacombe, M.; Gill, P. M. W.; Johnson, B.; Chen, W.; Wong, M. W.; Gonzalez, C.; and Pople, J. A. *Gaussian 03*, Revision C.02; Gaussian, Inc.: Wallingford CT, 2004.

31. Vlček, A.; Záliš, S. Modeling of Charge-Transfer Transitions and Excited States in d^6 Transition Metal Complexes by DFT Techniques. *Coordination Chemistry Reviews* **2007**, *251*, 258-287.

32. Cramer, C.J.; Truhlar, D.G. Density Functional Theory for Transition Metals and Transition Metal Chemistry. *Physical Chemistry Chemical Physics* **2009**, *11*, 10757-10816.

33. Fantacci, S.; De Angelis, F. A Computational Approach to the Electronic and Optical Properties of Ru(II) and Ir(III) Polypyridyl Complexes: Applications to DSC, OlED And NLO. *Coordination Chemistry Reviews* **2011**, *255*, 2704-2726.

34. Szabo, A.; Ostlund, N. S. *Modern Quantum Chemistry, 1st edition (revised)*; McGraw-Hill, Inc.: New York, NY, USA, 1989.

35. Jensen, F. *Introduction to Computational Chemistry, 2nd edition*; John Wiley & Sons Ltd: West Sussex, England, 2008.

36. Slater, J. C. The Theory of Complex Spectra. *Physical Review* **1929**, *34*, 1293-1322.

37. Baerends, E. J.; Gritsenko, O. V. A Quantum Chemical View of Density Functional Theory. *Journal of Physical Chemistry A* **1997**, *101*, 5383-5403.

38. Piela, L. *Ideas of Quantum Chemistry, 1st edition*; Elsevier Science Limited: Amsterdam, The Netherlands, 2007.

39. Hohenberg, P.; Kohn, W. Inhomogeneous Electron Gas. *Physical Review B* **1964**, *136*, 864.

40. Kohn, W.; Sham, L. J. Self-consistent Equations Including Exchange and Correlation Effects. *Physical Review* **1965**, *140*, 1133-1138.

41. Becke, A. D. Density-Functional Thermochemistry. III. The Role of Exact Exchange. *Journal of Chemical Physics* **1993**, *98*, 5648-5652.

42. Koch, W.; Holthausen, M. C. *A Chemist's Guide to Density Functional Theory, 2nd edition*; WILEY-VCH Verlag GmbH: Weinheim, Germany, 2000.

43. Dreuw, A.; Head-Gordon, M. Single-reference ab initio Methods for the Calculation of Excited States of Large Molecules. *Chemical Reviews* **2005**, *105*, 4009-4037.

44. Lee, S. S.; Loo, Y.-L. Structural Complexities in the Active Layers of Organic Electronics. *Annual Review of Chemical and Biomolecular Engineering* **2010**, *1*, 59-78.

45. Facchetti, A. π-Conjugated Polymers for Organic Electronics and Photovoltaic Cell Applications. *Chemistry of Materials* **2011**, *23*, 733-758.

46. Cataldo, S.; Pignataro, B. Polymeric Thin Films for Organic Electronics: Properties and Adaptive Structures. *Materials* **2013**, *6*, 1159-1190.

47. Brabec, C. J. Organic Photovoltaics: Technology and Market. *Solar Energy Materials and Solar Cells* **2004**, *83*, 273-292.

48. Loo, Y.-L.; McCulloch, I. Progress and Challenges in Commercialization of Organic Electronics. *MRS Bulletin* **2008**, *33*, 653-662.

49. Krebs, F. C. Fabrication and Processing of Polymer Solar Cells: A Review of Printing and Coating Techniques. *Solar Energy Materials & Solar Cells* **2009**, *93*, 394-412.

50. Medford, A.J.; Lilliedal, M. R.; Jørgensen, M.; Aaro, D.; Pakalski, H.; Fyenbo, J.; Krebs, F. C. Grid-connected Polymer Solar Panels: Initial Considerations of Cost, Lifetime, and Practicality. *Optics Express* **2010**, *18*, A272-A285.

51. Jørgensen, M.; Norrman, K.; Krebs, F. C. Stability/degradation of polymer solar cells. *Solar Energy Materials and Solar Cells* **2008**, *92*, 686-714.

52. Green, M. A.; Emery, K.; Hishikawa, Y.; Warta, W.; Dunlop, E. D. Solar Cell Efficiency Tables (Version 39). *Progress in Photovoltaics* **2012**, *20*, 12-20.

53. Deibel, C.; Strobel, T.; Dyakonov, V. Role of the Charge Transfer State in Organic Donor-Acceptor Solar Cells. *Advanced Materials* **2010**, *22*, 4097-4111.

54. Park, S. H.; Roy, A.; Beaupre, S.; Cho, S.; Coates, N.; Moon, J. S.; Moses, D.; Leclerc, M.; Lee, K.; Heeger, A. J. Bulk Heterojunction Solar Cells with Internal Quantum Efficiency Approaching 100%. *Nature Photonics* **2009**, *3*, 297–303.

55. Etzold, F.; Howard, I. A.; Mauer, R; Meister, M; Kim, T.-D.; Lee, K.-S.; Baek, N. S.; Laquai, F. Ultrafast Exciton Dissociation Followed by Nongeminate Charge Recombination in PCDTBT:PCBM Photovoltaic Blends. *Journal of American Chemical Society* **2011**, *133*, 9469–9479.

56. Brabec_ChemSocRev_2011 Brabec, C. J.; Heeney, M.; McCulloch, I.; Nelson, J. Influence of Blend Microstructure on Bulk Heterojunction Organic Photovoltaic Performance. *Chemical Society Reviews* **2011**, *40*, 1185-1199.

57. Chen, J.-W.; Cao, Y. Development of Novel Conjugated Donor Polymers for High-Efficiency Bulk-Heterojunction Photovoltaic Devices. *Accounts of Chemical Research* **2009**, *42*, 1709-1718.

58. Zhan, X.-W.; Zhu, D.-B. Conjugated Polymers for High-Efficiency Organic Photovoltaics. *Polymer Chemistry* **2010**, *1*, 409-419.

59. Son, H. J.; He, F.; Carsten, B.; Yu, L.-P. Are We There Yet? Design of Better Conjugated Polymers for Polymer Solar Cells. *Journal of Materials Chemistry* **2011**, *21*, 18934-18945.

60. Inganäs, O.; Zhang, F.; Tvingstedt, K.; Andersson, L. M.; Hellström, S.; Andersson, M. R. Polymer Photovoltaics with Alternating Copolymer/Fullerene Blends and Novel Device Architectures. *Advanced Materials* **2010**, *22*, E100-E116.

61. Schwartz, B. J. Conjugated Polymers as Molecular Materials: How Chain Conformation and Film Morphology Influence Energy Transfer and Interchain Interactions. *Annual Review of Physical Chemistry* **2003**, *54*, 141-172.

62. Jespersen, K. G.; Beenken, W. J. D.; Zaushitsyn, Y.; Yartsev, A.; Andersson, M.; Pullerits, T.; Sundström, V. The Electronic States of Polyfluorene Copolymers with Alternating Donor-Acceptor Unit. *Journal of Chemical Physics* **2004**, *121*, 12613-12617.

63. Clarke, T. M.; Durrant, J. R. Charge Photogeneration in Organic Solar Cells. *Chemical Reviews* **2010**, *110*, 6736-6767.

64. Goris, L.; Haenen, K.; Nesladek, M.; Wagner, P.; Vanderzande, D.; De Schepper, L.; D'Haen, J.; Lutsen, L.; Manca, J. V. Absorption Phenomena in Organic Thin Films for Solar Cell Applications Investigated by Photothermal Deflection Spectroscopy. *Journal of Materials Science* **2005**, *40*, 1413-1418.

65. Loi, M. A.; Toffanin, S.; Muccini, M.; Forster, M.; Scherf, U.; Scharber, M. Charge Transfer Excitons in Bulk Heterojunctions of a Polyfluorene Copolymer and a Fullerene Derivative. *Advanced Functional Materials* **2007**, *17*, 2111-2116.

66. Andersson, L. M.; Inganäs, O. From Short to Long - Optical and Electrical Transients in Photovoltaic Bulk Heterojunctions of Polyfluorene/fullerenes. *Chemical Physics* **2009**, *357*, 120-123.

67. Ponseca, C. S.; Yartsev, A.; Wang, E.; Andersson, M. R.; Vithanage, D.; Sundström, V. Ultrafast Terahertz Photoconductivity of Bulk Heterojunction Materials Reveals High Carrier Mobility up to Nanosecond Time Scale. *Journal of the American Chemical Society* **2012**, *134*, 11836-11839.

68. Pivrikas, A.; Sariciftci, N. S.; Juska, G.; Österbacka, R. A Review of Charge Transport and Recombination in Polymer/Fullerene Organic Solar Cells. *Progress in Photovoltaics* **2007**, *15*, 677-696.

69. Piliego, C.; Loi, M. A. Charge Transfer State in Highly Efficient Polymer-Fullerene Bulk Heterojunction Solar Cells. *Journal of Materials Chemistry* **2012**, *22*, 4141-4150.

70. Bakulin, A. A.; Rao, A.; Pavelyev, V. G.; van Loosdrecht, P. H. M.; Pshenichnikov, M. S.; Niedzialek, D.; Cornil, J.; Beljonne, D.; Friend, R. H. The Role of Driving Energy and Delocalized States for Charge Separation in Organic Semiconductors. *Science* **2012**, *335*, 1340-1344.

71. Grancini, G.; Maiuri, M.; Fazzi, D.; Petrozza, A.; Egelhaaf, H.-J.; Brida, D.; Cerullo, G.; Lanzani, G. Hot Exciton Dissociation in Polymer Solar Cells. *Nature Materials* **2013**, 12, 29-33.]

72. De, S.; Pascher, T.; Maiti, M.; Jespersen, K. G.; Kesti, T.; Zhang, F.; Inganäs, O.; Yartsev, A.; Sundström, V. Geminate Charge Recombination in Alternating Polyfluorene Copolymer/Fullerene Blends. *Journal of American Chemical Society* **2007**, *129*, 8466-8472.

73. Lee, J.; Vandewal, K.; Yost, S. R.; Bahlke, M. E.; Goris, L.; Baldo, M. A.; Manca, J. V.; Van Voorhis, T. Charge Transfer State Versus Hot Exciton Dissociation in Polymer-Fullerene Blended Solar Cells. *Journal of American Chemical Society* **2010**, 132, 11878-11880.

74. Singh, S.; Pandit, B.; Hukic-Markosian, G.; Basel, T. P.; Vardeny, Z. V.; Li, S.; Laird, D. Ultrafast Transient Spectroscopy of Nano-Domains of Polymer/Fullerene Blend for Organic Photovoltaic Applications. *Journal of Applied Physics* **2012**, *112*, 123505.

75. Tvingstedt, K.; Vandewal, K.; Gadisa, A.; Zhang, F.; Manca, J. V.; Inganäs, O. Electroluminescence from Charge Transfer States in Polymer Solar Cells. *Journal of American Chemical Society* **2009**, *131*, 11819-11824.

76. Veldman, D; Ipek, Ö; Meskers, S. C. J.; Sweelssen, J; Koetse, M. M.; Veenstra, S. C.; Kroon, J. M.; van Bavel, S. S.; Loos, J; Janssen, R. A. J. Compositional and Electric Field Dependence of the Dissociation of Charge Transfer Excitons in

Alternating Polyfluorene Copolymer/Fullerene Blends. *Journal of American Chemical Society* **2008**, *130*, 7721-7735.

77. De, S.; Kesti, T.; Maiti, M.; Zhang, F.; Inganäs, O.; Yartsev, A.; Pascher, T.; Sundström, V. Exciton Dynamics in Alternating Polyfluorene/Fullerene Blends. *Chemical Physics* **2008**, *350*, 14-22.

78. Zhang, F.; Bijleveld, J.; Perzon, E.; Tvingstedt, K.; Barrau, S.; Inganäs, O.; Andersson, M. R. High Photovoltage Achieved in Low Band Gap Polymer Solar Cells by Adjusting Energy Levels of a Polymer With the LUMOs of Fullerene Derivatives. Journal of Materials Chemistry **2008**, *18*, 5468-5474.

79. Jarzab, D.; Cordella, F.; Gao, J.; Scharber, M.; Egelhaaf, H.-J.; Loi, M. A. Low-Temperature Behaviour of Charge Transfer Excitons in Narrow-Bandgap Polymer-Based Bulk Heterojunctions. *Adanced Energy Materials* **2011**, *1*, 604–609.

80. Andersson, L. M.; Zhang, F.; Inganäs, O. Stoichiometry, Mobility, and Performance in Bulk Heterojunction Solar Cells. *Applied Physics Letters* **2007**, *91*, 071108.

81. Servaites, J. D.; Savoie, B. M.; Brink, J. B.; Marks, T. J.; Ratner, M. A. Modeling Geminate Pair Dissociation in Organic Solar Cells: High Power Conversion Efficiencies Achieved with Moderate Optical Bandgaps.

82. Coe, B. J.; Curati, N. R. M. Metal Complexes for Molecular Electronics and Photonics. *Comments on Inorganic Chemistry* **2004**, *25*, 147-184.

83. Bruijnincx, P. C. A.; Sadler, P. J. New Trends for Metal Complexes with Anticancer Activity. *Current Opinion in Chemical Biology* **2008**, *12*, 197-206.

84. Wagenknecht, P. S.; Ford, P. C. Metal Centered Ligand Field Excited States: Their Roles in the Design and Performance of Transition Metal Based Photochemical Molecular Devices. *Coordination Chemistry Review* **2011**, *255*, 591-616.

85. Sauvage, J. P.; Collin, J. P.; Chambron, J. C.; Guillerez, S.; Coudret, C.; Balzani, V.; Barigelletti, F.; Decola, L.; Flamigni, L. Ruthenium(II) and Osmium(II) Bis(Terpyridine) Complexes in Covalently-linked Multicomponent Systems - Synthesis, Electrochemical-Behavior, Absorption-Spectra, and Photochemical and Photophysical Properties. *Chemical Reviews* **1994**, *94*, 993-1019.

86. Barigelletti, F.; Flamigni, L. Photoactive molecular wires based on metal complexes. *Chemical Society Reviews* **2000**, *29*, 1-12.

87. Sun, L. C.; Hammarström, L.; Åkermark, B.; Styring, S. Towards Artificial Photosynthesis: Ruthenium-Manganese Chemistry for Energy Production. *Chemical Society Reviews* **2001**, *30*, 36-49.

88. Vlček, A. The Life and Times of Excited States of Organometallic snd Coordination Compounds. *Coordination Chemistry Reviews* **2000**, *200*, 933-977.

89. Juris, A.; Balzani, V.; Barigelletti, F.; Campagna, S.; Belser, P.; Vonzelewsky, A. Ru(II) Polypyridine Complexes - Photophysics, Photochemistry, Electrochemistry, and Chemi-Luminescence. *Coordination Chemistry Review* **1988**, *84*, 85-277.

90. Huheey, J. E.; Keiter, E. A.; Keiter, R. L. *Inorganic Chemistry. Principles of Structure and Reactivity, 4th edition*; HarperCollins College Publishers: New York, NY, USA, 1993.

91. Hecker, C. R.; Gushurst, A. K. I.; McMillin, D. R. Phenyl Substituents and Excited-State Lifetimes in Ruthenium(II) Terpyridyls. *Inorganic Chemistry* **1991**, *30*, 538-541.

92. Medlycott, E. A.; Hanan, G. S. Synthesis and Properties of Mono- and Oligo-Nuclear Ru(II) Complexes of Tridentate Ligands: The Quest for Long-lived Excited States at Room Temperature. *Coordination Chemistry Reviews* **2006**, *250*, 1763-1782.

93. Wolpher, H.; Johansson, O.; Abrahamsson, M.; Kritikos, M.; Sun, L. C.; Åkermark, B. A Tridentate Ligand for Preparation of Bisterpyridine-Like Ruthenium(II) Complexes with an Increased Excited State Lifetime. *Inorganic Chemistry Communications* **2004**, *7*, 337-340.

94. Abrahamsson, M.; Wolpher, H.; Johansson, O.; Larsson, J.; Kritikos, M.; Eriksson, L.; Norrby, P.-O.; Bergquist, J.; Sun, L. C.; Åkermark, B.; Hammarström, L. A New Strategy for the Improvement of Photophysical Properties in Ruthenium(II) Polypyridyl Complexes. Synthesis and Photophysical and Electrochemical Characterization of Six Mononuclear Ruthenium(II) Bisterpyridine-Type Complexes. *Inorganic Chemistry* **2005**, *44*, 3215-3225.

95. Abrahamsson, M.; Becker, H.-C.; Hammarström, L.; Bonnefous, C.; Chamchoumis, C.; Thummel, R. P. Six-membered Ring Chelate Complexes of Ru(II): Structural and Photophysical Effects. *Inorganic Chemistry* **2007**, *46*, 10354-10364.

96. Abrahamsson, M.; Jäger, M.; Österman, T.; Eriksson, L.; Persson, P.; Becker, H.-C.; Johansson, O.; Hammarström, L. A 3.0 μs Room Temperature Excited State Lifetime of a Bistridentate RuII-Polypyridine Complex for Rod-like Molecular Arrays. *Journal of the American Chemical Society* **2006**, *128*, 12616-12617.

97. Schramm, F.; Meded, V.; Fliegl, H.; Fink, K.; Fuhr, O.; Qu, Z.-R. Klopper, W.; Finn, S.; Keyes, T. E.; Ruben, M. Expanding the Coordination Cage: A Ruthenium(II)-Polypyridine Complex Exhibiting High Quantum Yields under Ambient Conditions. *Inorganic Chemistry* **2009**, *48*, 5677-5684.

98. Brown, D. G.; Sanguantrakun, N.; Schulze, B.; Schubert, U. S.; Berlinguette, C. P. Bis(tridentate) Ruthenium-Terpyridine Complexes Featuring Microsecond Excited-State Lifetimes. *Journal of the American Chemical Society* **2012**, *134*, 12354-12357.

99. Dinda, J.; Liatard, S.; Chauvin, J.; Jouvenot, D.; Loiseau, F. Electronic and Geometrical Manipulation of the Excited State of Bis-Terdentate Homo- and Heteroleptic Ruthenium Complexes. *Dalton Transactions* **2011**, *40*, 3683-3688.

100. Borg, O. A.; Godinho, S. S. M. C.; Lundqvist, M. J.; Lunell, S.; Persson, P. Computational Study of The Lowest Triplet State of Ruthenium Polypyridyl

Complexes Used in Artificial Photosynthesis. *Journal of Physical Chemistry A* **2008**, *112*, 4470-4476.

101. Alary, F.; Heully, J.-L.; Bijeire, L.; Vicendo, P. Is the ^{3}MLCT the Only Photoreactive State of Polypyridyl Complexes? *Inorganic Chemistry* **2007**, *46*, 3154-3165.

102. Abrahamsson, M.; Lundqvist, M.J.; Wolpher, H.; Johansson, O.; Eriksson, L.; Bergquist, J.; Rasmussen, T.; Becker, H.-C.; Hammarström, L.; Norrby, P.-O.; Akemark, B.; Persson, P. Steric Influence on the Excited-State Lifetimes of Ruthenium Complexes with Bipyridyl-Alkanylene-Pyridyl Ligands. *Inorganic Chemistry* **2008**, *47*, 3540-3548.

103. Chou, P.-T.; Chi, Y.; Chung, M.-W.; Lin, C.-C. Harvesting Luminescence via Harnessing the Photophysical Properties of Transition Metal Complexes. *Coordination Chemistry Reviews* **2011**, *255*, 2653-2665.

104. Jakubikova, E.; Chen, W.-Z.; Dattelbaum, D. M.; Rein, F. N.; Rocha, R. C.; Martin, R. L.; Batista, E. R. Electronic Structure and Spectroscopy of $[Ru(tpy)_2]^{2+}$, $[Ru(tpy)(bpy)(H_2O)]^{2+}$, and $[Ru(tpy)(bpy)(Cl)]^{+}$. *Inorganic Chemistry* **2009**, *48*, 10720-10725.

105. Dixon, I. M.; Alary, F.; Heully, J.-L. Electronic Peculiarities of the Excited States of $[RuN_5C]^{+}$ vs. $[RuN_6]^{2+}$ Polypyridine Complexes: Insight from Theory. *Dalton Transactions* **2010**, *39*, 10959-10966.

106. Piau, R. E.; Guillon, T.; Lebon, E.; Perrot, N.; Alary, F.; Boggio-Pasqua, M.; Heully, J.-L.; Juris, A.; Sutra, P.; Igau, A. Photophysical and Electrochemical Properties of Polypyridine Imine Ruthenium(II) Complexes: A Comparative Experimental and Theoretical Study. *New Journal of Chemistry* **2012**, *36*, 2484-2492.

107. Alary, F.; Boggio-Pasqua, M.; Heully, J.-L.; Marsden, C. J.; Vicendo, P. Theoretical Characterization of the Lowest Triplet Excited States of the Tris-(1,4,5,8-Tetraazaphenanthrene) Ruthenium Dication Complex. *Inorganic Chemistry* **2008**, *47*, 5259-5266.

108. Salassa, L.; Garino, C.; Salassa, G.; Gobetto, R.; Nervi, C. Mechanism of Ligand Photodissociation in Photoactivable $[Ru(bpy)_2L_2]^{2+}$ Complexes: A Density Functional Theory Study. *Journal of the American Chemical Society* **2008**, *130*, 9590-9597.

109. Salassa, L.; Garino, C.; Salassa, G.; Nervi, C.; Gobetto, R.; Lamberti, C.; Gianolio, D.; Bizzarri, R.; Sadler, P.J. Ligand-Selective Photodissociation from $[Ru(bpy)(4AP)_4]^{2+}$: A Spectroscopic and Computational Study. *Inorganic Chemistry* **2009**, *48*, 1469-1481

110. Heully, J.-L.; Alary, F.; Boggio-Pasqua, M. Spin-orbit effects on the photophysical properties of $Ru(bpy)_3^{2+}$. *Journal of Chemical Physics* **2009**, *131*, 184308.

111. Lebon, E.; Bastin, S.; Sutra, P.; Vendier, L.; Piau, R. E.; Dixon, I. M.; Boggio-Pasqua, M.; Alary, F.; Heully, J.-L.; Igau, A.; Juris, A. Can a Functionalized Phosphine Ligand Promote Room Temperature Luminescence of the [Ru(bpy)(tpy)] $^{2+}$ core? *Chemical Communications* **2012**, *48*, 741-743.

112. Yang, L.; Okuda, F.; Kobayashi, K.; Nozaki, K.; Tanabe, Y.; Ishii, Y .; Haga, M.-A. Syntheses And Phosphorescent Properties Of Blue Emissive Iridium Complexes With Tridentate Pyrazolyl Ligands. *Inorganic Chemistry* **2008**, *47*, 7154-7165.

113. Guillon, T.; Boggio-Pasqua, M.; Alary, F.; Heully, J.-L.; Lebon, E.; Sutra, P.; Igau, A. Theoretical Investigation on the Photophysical Properties of Model Ruthenium Complexes with Diazabutadiene Ligands $[Ru(bpy)_{3-x}(dab)_x]^{2+}$ (x=1-3). *Inorganic Chemistry* **2010**, *49*, 8862-8872.

114. Hewitt, J. T.; Vallett, P. J.; Damrauer, N. H. Dynamics of the ^{3}MLCT in R(II) Terpyridyl Complexes Probed by Ultrafast Spectroscopy: Evidence of Excited-State Equilibration and Interligand Electron Transfer. *Journal of Physical Chemistry A* **2012**, *116*, 11536-11547.

115. Thompson, D. W.; Fleming, C. N.; Myron, B. D.; Meyer, T. J. Rigid Medium Stabilization of Metal-to-ligand Charge Transfer Excited States. *Journal of Physical Chemistry B* **2007**, *111*, 6930-6941.

116. Terence, J. K. Luminescence Kinetics of Metal Complexes in Solution. *Progress in Reaction Kinetics* **1980**, *10*, 301-398.

117. Abrahamsson, M. Tuning of the Excited State Properties of Ruthenium(II)-Polypyridyl Complexes. Ph.D. Dissertation, Uppsala University, Sweden, December 1, 2006.